POLITECNICO DI TORINO

Master's degree in aerospace engineering

Master's degree thesis

Optimization of interplanetary trajectories to near-Earth asteroids using electric propulsion

Supervisor
Prof. Lorenzo Casalino

Candidate
Ivan Felli

July 2022

Abstract

In this thesis a strategy of optimization of missions towards Near-Earth asteroids using electric propulsion will be analyzed. Near-Earth asteroids, or NEA, are a class of asteroids characterized by being very close to the Earth, and this aspect makes them extremely interesting, firstly in order to monitor their positions and predict eventual potential impacts with Earth and, secondly, since it is meaningful to study and determine their physical characteristics so that it will be possible to deduce much information about the origin of life on our planet, also taking into account the rate at which new ones are discovered, thanks to sky observations. In this sense, employing electric propulsion is convenient, given that it is distinguished by a sensibly lower propellant consumption, if compared with chemical propulsion, with a consequent substantial saving in terms of mission costs.

The work specifically focuses on the simulation of missions toward ten of these asteroids, from which it is possible to discriminate two different maneuver strategies, each one with different characteristics. The final goal of this thesis consists in determining the causes that make one more convenient than the other, depending on the asteroid taken into consideration, which means that some hypotheses will be formulated and then properly tested using counterproofs, thus entailing the simulation of missions toward the same asteroids while fictitiously modifying the orbital parameters of the asteroids themselves. In order to optimize the trajectories of the missions, the theory of optimal control will be applied, using indirect methods of resolution of the fundamental equations, which are characterized by a significant numeric precision, with a low number of parameters and limited time of calculation.

Acknowledgements

Contents

List of Figures

List of Tables

Chapter 1

Introduction

1.1 Thesis overview and objectives

In this thesis, the results of simulations investigating the possibility of optimization of missions toward Near-Earth asteroids will be presented and commented. The whole work is divided into chapters, each focusing on one particular aspect of the work itself. In particular, in *Chapter 1* the base concepts and meaning of spacecraft trajectory optimization will be given, while the destination of the missions will be described in *Chapter 2*. In *Chapter 3* and *Chapter 4* the physics of astrodynamics and mathematics of indirect optimization, together with the theory of optimal control, which are the basis of the simulations, will be presented. *Chapter 5* and *Chapter 6* are central, as the equation solved in the simulation and the method applied to get to the results are there introduced. The results of the simulation, with comments and observations, are the central point of *Chapter 7*. At last, the conclusion and the recap of the work are reported in the last chapter, the *Chapter 8*.

1.2 What is spacecraft trajectory optimization

The spacecraft trajectory optimization problem can be defined as a process of research of a trajectory that satisfies specific criteria, including initial and final conditions. This process can be divided into four main parts, which are:

- defining the mathematical model of the system dynamics;

- defining appropriate objectives;

- developing an approach;

- achieving the solution.

Each one of these intermediate phases leads to the definition of: *model*, *objective*, *approach* and *solution*, respectively.

Moreover, each space mission includes several components and peculiar aspects, such as mission requirements, goals, expected accuracy, desired convergence, mission plan, and so on. These last aspects, therefore, affect the definition of the aforementioned steps differently.

The definition of the process follows a specific sequence of steps, the first one of which deals with the understanding of the dynamics inherent in the system. This means we need to state

a mathematical model which completely describes the system itself, thus choosing a series of state variables and deriving the motion equations for the spacecraft.

The second step is centered on mission objectives and, to this aim, cost functions are introduced. We basically have two categories for this step, one according to the type of objectives and a second one according to the number of objectives.

The third step is represented by the methods and techniques employed to solve the trajectory design problem. In this phase, two main ways are possible, which are the analytical and numerical approaches. The analytical approach is mainly based on the theory of optimal control, which will be central in this work. The aim of this theory is to determine a time history of controls that satisfies the constraints given by the physics of the problem while maximizing a specific performance index. All the methods usually applied in trajectory optimization can be collected into two main categories: the *direct methods* and the *indirect methods*. The first ones attempt to find the minimum value of a cost function by taking into account state vectors and input vectors, while the second ones exploit adjoint equations together with state and input vectors given by the Pontryagin's Principle.

The fourth step involves the resolution of the problem obtained in the previous phase. So, if the developed approach is an analytical one, the solution will likely be a closed-form analytical solution, even though, if the numerical approach is adopted, the problem will be a black-box optimization problem, thus needing a numerical algorithm to get the solution. However, most of the optimization problems are solved by a numerical technique. The reason is that this type of mathematical problem does not have a closed-form solution, because of its nonlinearity properties, unless specific assumptions are considered, which may affect the physical meaning of the simulation.
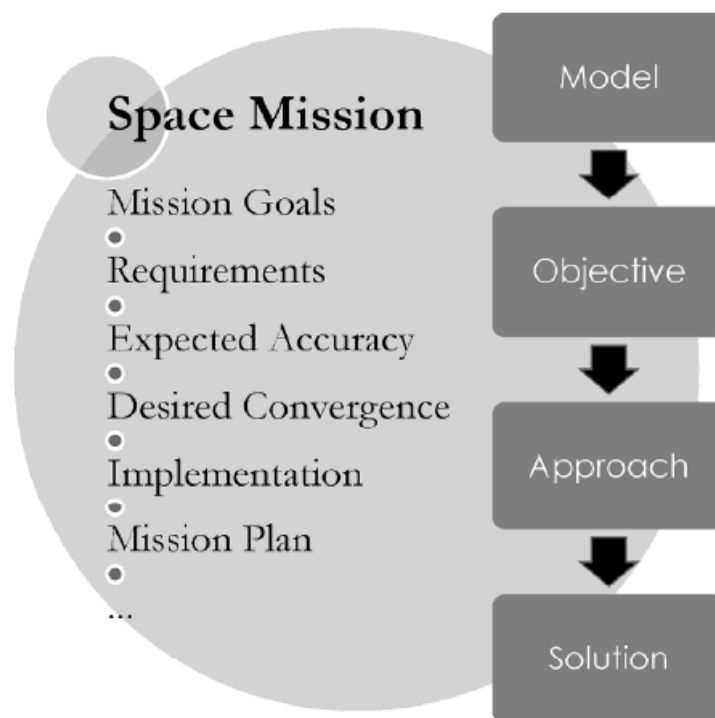
Figure 1.1: Flow chart of a space trajectory optimization process.

The definition of a spacecraft trajectory model is based on a set of ordinary differential equations

describing the evolution in time of position and velocity of the spacecraft itself. It is possible to describe this set of equations as follows:

$$\dot{\vec{x}} = f(\vec{x}(t), \vec{u}(t), t) \tag{1.1}$$

where t represents the time, $\vec{x}$ is an n-dimensional vector containing the state variables and $\vec{u}(t)$ is an m-dimensional vector including the components of the control vector, which serves as the system input.

Depending on the type of space mission, we can have an *impulsive* or a *continuous model*:

- the impulsive model is the traditional model used in astrodynamics to simulate spacecraft maneuvers. In this model, the inputs are supposed to be zero $u = 0$ and the increments of velocity Δv are assumed to occur instantaneously, thus with a burning time $\Delta t = 0$. This model usually fits in cases when high thrust levels and low specific impulse (with consequent high velocity variations) are considered. Thrust phases in impulsive models are short if compared to the mission's duration, therefore thrust arcs are modeled as isolated or, in other words, as a simple discontinuity of velocity;

- the continuous model, conversely, is characterized by a non-zero input ($u \neq 0$) which leads to a more precise but also more onerous simulation in terms of calculation. The continuous model is particularly adequate for low-thrust missions as, in these cases, the transfer time raises remarkably.

In addition to the mathematical model, the representation of the dynamics of the spacecraft motion can lead to a new categorization of the models. In fact, we can have two main categories, corresponding to the *two-body problem* and the *N-body problem*. In both cases, it is possible to assume either the impulsive or the continuous model.

Another key aspect of spacecraft trajectories optimization is the definition of objectives depending on the mission's requirements. These objectives are defined by functions, such as cost functions, in the optimal control field, which may be fuel mass, total velocity increment, state variables errors, acceleration, or final spacecraft mass, which is related to fuel saving, as assumed in this work.

COST FUNCTION $\rightarrow J = h(\vec{x}(t_f), t_f) + \int_{t_0}^{t_f} g(\vec{x}(t), \vec{u}(t), t)dt$

DYNAMIC EQUATION $\rightarrow \dot{\vec{x}} = f(\vec{x}(t), \vec{u}(t), t)$

INITIAL BOUNDARY CONDITION $\rightarrow \vec{x}(t_0) = \vec{x}_0$

TERMINAL BOUNDARY CONDITION $\rightarrow \psi(\vec{x}(t_f)) = 0$

PATH CONSTRAINTS $\rightarrow \phi_l < \phi(x(t), u(t)) < \phi_u$
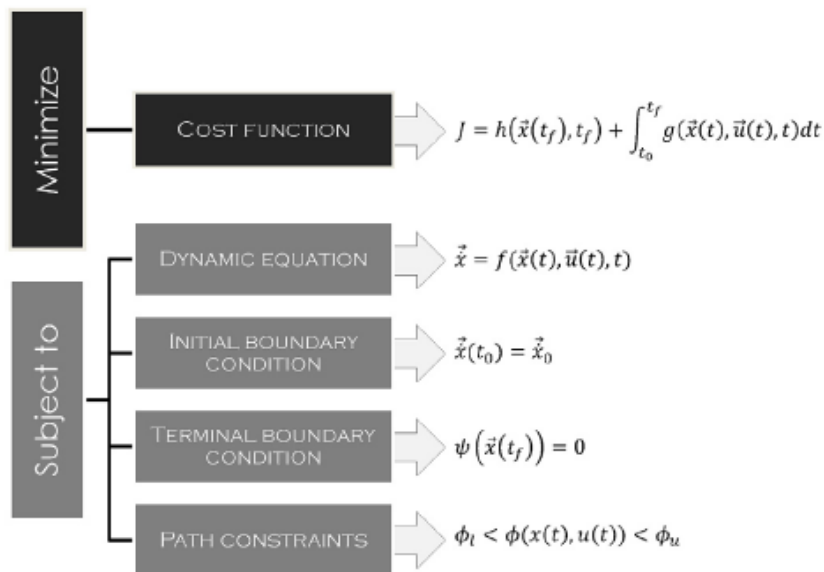
Figure 1.2: Definition of a optimum problem.

The general form of cost function, also known as Bolza cost function, as reported down below:

$$J(\vec{x}, \vec{u}, t) = h(\vec{x}(t_f), t_f) + \int_{t_0}^{t_f} g(\vec{x}(t), \vec{u}(t), t) dt \tag{1.2}$$

with t_0 and t_f initial and final times, respectively. The function h represents the Mayer term which defines the cost related to the final states, while the function g is called the Lagrange term or the running cost which determines the state and control costs. The objective function can include only the Mayer term, only the Lagrange term, or both, depending on the variable being optimized in the mission.

One possible type of objective is related to the Mayer term in the equation above, which is a function of state variables at the end of the mission. We can choose variables such as:

- time, that is the final time of the mission, related to the mission duration, mathematically expressed as: $J = t_f$

- velocity increment, which represent a cost in space propulsion, thus it is convenient to minimize it. In formula: $J = \sum_{i=0}^{n} |\Delta v_i|$;

- initial and terminal conditions, which are typically seen as constraints, even though in some optimization processes, they are objectives express by the formalism: $J = \phi(\vec{x}(t_0), \vec{x}(t_f))$, where ϕ contains the initial and final constraint.

Alternatively, we have types of objective that are related to the Lagrange term, like:

- acceleration, which is, analogously to the velocity variation, a cost in term of fuel, thus, the cost function will be $J = \frac{1}{2} \int_{t_0}^{t_f} \gamma^2 dt$

- fuel mass, which can be considered, besides velocity increment and acceleration, a representation of spent energy, therefore the expression of cost function will be: $J = \int_{t_0}^{t_f} m_{fuel} dt$ or, if transfer time and mass decreasing rate are fixed: $J = m_{fuel}$.

In our case, the control variable will be the final mass of the spacecraft, whose value has to be maximum:

$$J = m_f \tag{1.3}$$

In order to solve the characteristic equations, two types of approaches are possible: *analytical approaches* and *numerical approaches*.

Analytical approaches are the ideal ones as they provide solutions based on mathematical representation with a null approximation. Nevertheless, most of the time, they are not feasible because of the complexity of the problem itself.

Numerical approaches can be divided into two main branches, both of them attempting to minimize cost functions, limiting constraints violations by discrete approximations:

- **direct methods**, which allow to find the solution in a approximate way, by parameterizing the state variables $x(t)$ and the control inputs $u(t)$. This parametrization process usually implies a discretization process, therefore the equation, and thus the variables, defining the mathematical problem are transformed from continuous in time into discrete. These methods make the solutions more likely to be found but their optimality is not guaranteed;

- **indirect methods** exploit the same techniques and concepts as the direct methods but, in addition, they necessarily include analytic conditions of optimality. Therefore, they transform an optimization problem into the calculation of some parameters, called Lagrange multipliers or adjoint variables, with which the optimum conditions are fulfilled at the beginning and at the end of the process. It is important to notice that these adjoint variables evolve along the trajectory coherently with the state variables. Moreover, the domain of solution research in these methods based on Pontryagin's principle are made more complex by the fact that the adjoint variables range in unbounded set. In addition to that, indirect methods have weak robustness.
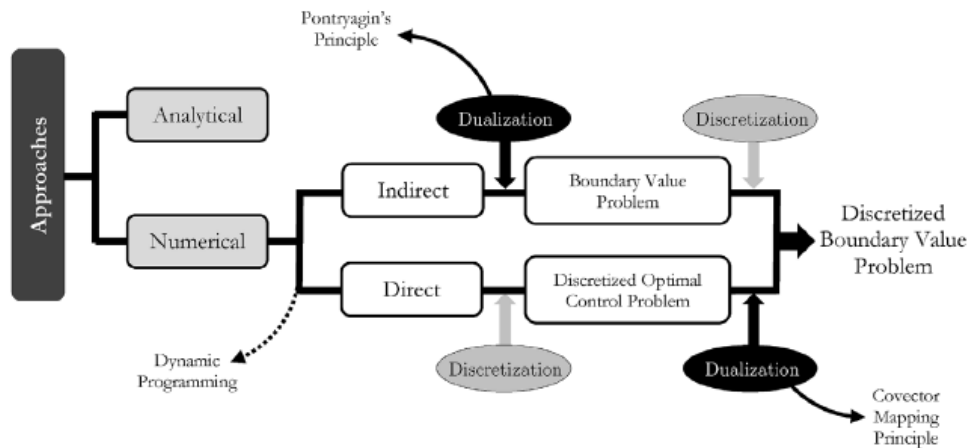
Figure 1.3: Methods of resolution of an optimum problem.

In conclusion, we can state that the main difference between direct and indirect methods lies in the introduction of the adjoint variables, limited to the indirect ones. One problem related to the indirect methods is difficulty related to the initial guess, as it is, a priori, unknown. [1] [2] [3]

Chapter 2

Scientific objective: Near-Earth asteroids

Near-Earth asteroids, also called NEAs, are a subgroup of celestial bodies being part of the larger category of Near-Earth objects (NEO). Near-Earth asteroids are those NEOs characterized by orbits that bring them to within a distance of 195 million kilometers from Earth, which means they can circulate through the Earth's orbital neighborhood, and their size can range from a few meters to nearly 40 kilometers. Most of NEAs are located in orbits that don't bring them very close to Earth, therefore they don't pose any risk of impact, but a small fraction of them, called potentially hazardous asteroids, are getting more attention, as in their case the risk is not close enough to zero. These last ones are defined as asteroids whose size reaches 140 meters and they orbit around the Sun at a distance from Earth of approximately 7.5 million kilometers.[4]

After the detection of the first NEO in history in 1898, later denominated 433 Eros, by Gustav Witt, the existence of a new population of asteroid-like bodies on orbits intersecting those of the inner planets was established.

Figure 2.1: 433 Eros, the first discovered NEA. [9]

Since that time an increasing number of NEOs were discovered, leading to an exponential

amount of known objects in our days. Nevertheless, the origin of these last ones was not clear at all, as the mechanism that led them to move from an orbit bounded by Mars and Jupiter, typical of the main asteroid belt, to a planet-crossing orbit was not explainable. It has been hypothesized that some of them may be formed by primordial matter, which went through a long journey from the earliest stages of the Solar System to our era, while the majority of them are fragments of asteroids from the Main Belt, originated by catastrophic collisions occurred in the past. Therefore, NEAs are getting more and more attention for several reasons. Firstly, from the purely scientific point of view, mostly because of their planets' crossing orbits, but also their lifetime, their possible genetic correlation with comets and meteorites, which are part of the huge problem of the origin of the Solar System, as well as the birth of life in the Universe. The second important aspect regarding NEAs is related to the continuation of civilization. In fact, these objects are believed to be potential sources of resources in a near-Earth environment, like metals and raw materials in general, as it is evidence they may contain volatile compounds, such as hydrogen, nitrogen, carbon, oxygen, and organics, at a concentration over 100 times greater than in the most volatile-rich lunar material. The third aspect of the importance of NEA deals with the asteroid hazard problem. In fact, according to the last available estimates, over 1500 asteroids larger than 1 km and about 135,000 larger than 100 m cross the Earth's orbits while orbiting the Sun. A collision of any of them with the Earth would be catastrophic, putting life on our planet under a serious threat. In fact, there is evidence given by lunar and terrestrial craters that imply an intense event of bombing over the age of the Solar System, that highlights the fact that it may cause huge devastation to our biosphere. Therefore, a deep study of their physical properties, together with their trajectories is crucial in order to protect mankind.
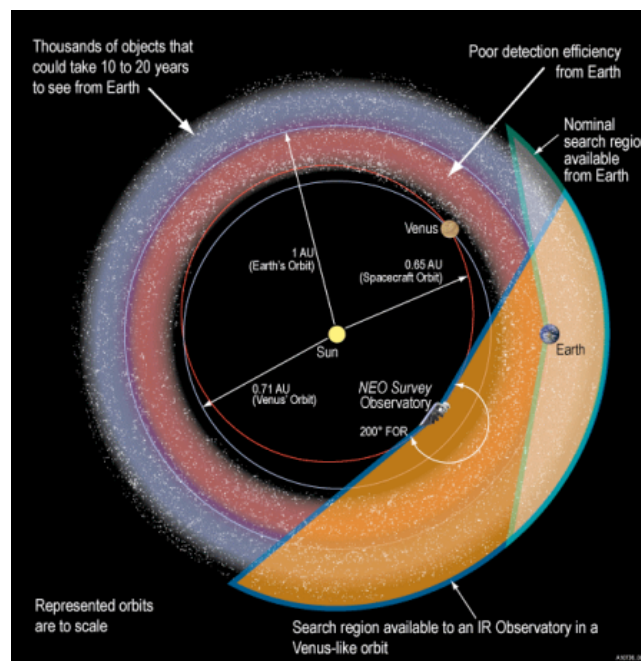
Figure 2.2: Distribution of NEAs in near-Earth environment.[8]

Near-Earth asteroids were divided into three groups: Atens, Apollos and Amors. In particular:

- **Aten asteroids** are defined as those NEAs whose orbits lie inside the Earth one, with a semi-major axis $a < 1AU$, and aphelion radii satisfying the relation $r_a \geq 0.983AU$, thus crossing Earth's orbit in their near-aphelia regions, as already discussed, given that the

current perihelion of Earth is roughly equal to $r_{aEarth} = 0.983 AU$;

- **Apollo asteroids** are characterized by two conditions regarding their semi-major axes and perihelion radii, in particular: $a \geq 1 AU$ and $r_p \leq 1.017 AU$. This means that they overlap Earth's orbit near their perihelia;

- **Amor asteroids** whose semi-major axes and perihelia radii are: $a \geq 1 AU$ and $1.017 AU < r_p \leq 1.3 AU$, then they do not overlap Earth's orbit, but only approach it.

Atens and Apollos are also called Earth-crossing asteroids (ECAs) for the aforementioned properties of crossing the Earth's orbit, with a shorter period (Aten group) and a longer period (Apollo group) than 1 year. Amors, on the other hand, as already said, do not cross Earth's orbit, but only approach it, even though secular variations of eccentricity and semi-major axis may cause part-time overlap. For the same causes, Apollos lose their overlap characteristic for a short period, thus becoming Amors asteroids.

Later analyses conducted by Rabinowitz suggested that two distinct population of NEAs can be distinguished: the first one corresponds to the above-mentioned Aten, Apollo and Amor group, while the second one is composed of a high number of small asteroids (less than 50 m in size) characterized by small eccentricities and inclinations, with semi-major axes $a \simeq 1$. These last ones determine a concentration of objects in the near-Earth space, also called the "near-Earth asteroid belt" that have perihelion radius $0.9 AU < r_p < 1.1 AU$ and aphelion radius $r_a < 1.4 AU$.

Another fundamental physical property of an NEA or, in general, of an asteroid, is its shape, as it is significant to investigate its origin and its collisional history. Near-Earth asteroids, in particular, are characterized by a large diversity in their shapes, from nearly spherical to highly elongated and irregular. The elongated shape can be easily explained noticing that most of the small NEAs are rubble pile asteroids, therefore, close interaction with a planet's gravity may lead to a distortion of the asteroid itself due to the tidal interaction, determining a cigar-like shape. This could explain the fact that this shape is very common in Near-Earth asteroids, rather than asteroids located in other regions.

Moreover, since NEAs have unstable orbits, they are often lost and replaced with tens of new objects. As a consequence, two main mechanisms have been proposed to explain the origin of new objects replacing the lost ones:

- The first mechanism assumes that NEAs are asteroidal fragments coming from the main-belt, formed by collisional processes and chaotic dynamics. Numerical evidence confirms this hypothesis, as it was shown that two regions in the main belt could have originated them, that are the regions affected by the resonance motion with Jupiter and the inner region of the main belt, causing chaotic increases in their orbital eccentricity, thus allowing them to cross planets' orbits;

- The second supposed sources for NEAs are extinct or dormant comets' nuclei. In fact, when a comet's nucleus depletes its volatile compounds, it originates an inert outer layer of material, called mantle or crust, that insulates the compounds lying in the inner part of the comet itself. At this point, the comet becomes inactive over a large region of its surface, making it quite indistinguishable from an asteroid.[5] [6] [7] [8]

The more likely hypothesis about the NEAs' origin is that these objects were removed from other regions of the Solar System by a sequence of collision and gravitational interactions with the planets, even causing a collision with the planets themselves. This last fact is confirmed by large craters on planets' surfaces, highlighting the importance these objects could have had in

the birth of life on our planet, also carrying important materials that allow the existence and the maintenance of the civilization on our planet.

Two more physical phenomena influence NEAs' orbits, causing a variation of their orbital parameters, which are the **Yarkovsky effect** and the **YORP effect**.
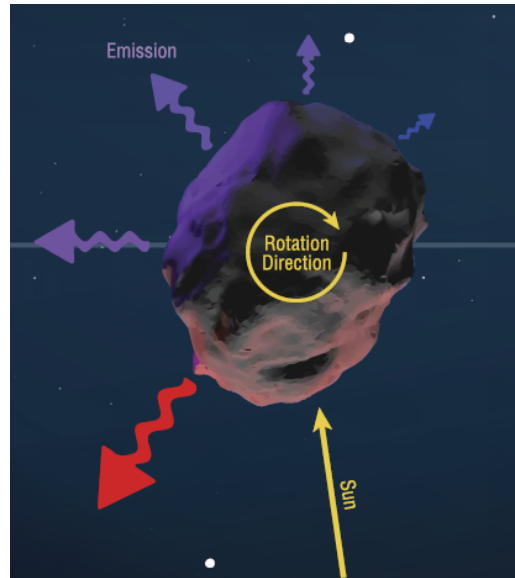
Figure 2.3: Scheme of Yarkovsky effect.[11]

- The **Yarkovsky effect** is the most significant nongravitational perturbation and it is due to radiative recoil of anisotropic thermal emission, leading asteroids to undergo a secular semi-major axis drift $\frac{da}{dt}$. Typical values of this variation of semi-major axis are around 10^{-4} to $10^{-3} AU/Myr$. This effect depends on several factors, such as the asteroid's spin rate, size, mass, shape, and thermal properties. Moreover, a key role is played by the asteroid's surface roughness, as it can enhance the semi-major axis drift by tens of percent. Therefore, the Yarkovsky effect is of vital importance to predict possible impacts on Earth;[10]

- The **YORP effect** (abbreviation for Yarkovsky–O'Keefe–Radzievskii–Paddack effect) is a phenomenon observable on spinning irregularly shaped asteroids, causing a variation of their spin rates and pole direction. It can be seen as an extension of the Yarkovsky effect to the spinning bodies, and it is caused by an asymmetric reflection, absorption, and IR re-emission of the sunlight by the asteroids themselves. Therefore, the YORP effect action mainly depends on the amount of solar energy received by the body, the insolation (therefore on the mean value of the inverse of the square of the distance of the asteroid from the Sun), its size and its albedo. In particular, the larger the amount of incoming energy is, the stronger this acceleration will be. In particular, this acceleration caused by the YORP torque can either continuously increase the rotation rate (spin-up) until a reshaping process occurring to the asteroid stops the angular acceleration and reverse the sign of spinning, or continuously decrease the rotation rate (spin-down) until the asteroid enters a tumbling rotation state. As mentioned, this acceleration is related also to the tendency to asymptotically shift the pole of the asteroid itself, as to make the axis perpendicular to the orbital plane. Its effect on the asteroids' spin rate is very weak, but it accumulates during the whole object's lifetime, thus causing a sensible variation of the spin rate. This phenomenon is particularly important for rubble pile asteroids, as it

can lead the asteroids themselves to undergo a process of mass shedding, also because of their high spin rates.[12] [13]

Chapter 3

Physical model

In this chapter, the basic concepts of the physics of the problem are reported. This thesis touches mainly two fundamental fields of physics: astrodynamics and electric propulsion, therefore a brief overview of notions needed to understand this work is given below.[14]

3.1 Fundamentals of astrodynamics

3.1.1 Universal law of gravitation

The starting point of mechanics of celestial bodies was given by Isaac Newton, who, after having enunciated the three laws of motion, formulated the law of universal gravitation, which states that any two bodies attract one another with a force that is directly proportional to the product of the two bodies' masses and inversely proportional to the square of the distance between one another.
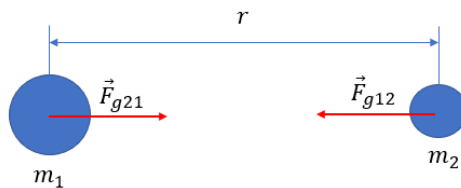
Figure 3.1: Scheme of gravitational interaction between two bodies.

In formula:

$$\vec{F}_g = -G\frac{m_1 m_2}{r^2}\frac{\vec{r}}{r} \tag{3.1}$$

where G is the universal gravitational constant and its value is equal to $G = 6.667 \times 10^{-11} Nm^2/kg^2$.

It is possible to make the problem more general by extending the formula written above to N masses. In the last case, each of the masses will attract all the others and will be attracted by all the others.
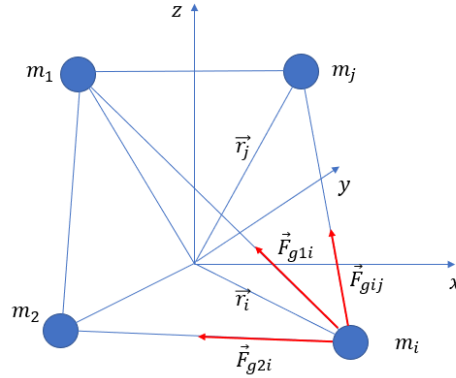
Figure 3.2: Scheme of N-body gravitational interaction

If we consider only one mass, the i-th mass, it is convenient to express this last case mathematically writing:

$$\vec{F}_g = -Gm_i \sum_{j=1,j\neq i}^{N} \frac{m_j}{r_{ij}^3}\vec{r}_{ij} \tag{3.2}$$

3.1.2 The two-body problem

The two-body problem is perhaps the most important concept of the whole celestial mechanics as, under certain simplifying assumptions and in the proximity of a very massive body, it allows to make calculations simple without introducing large errors. The simplifying assumptions are:

- the bodies are spherical and symmetric, as to consider bodies' masses as concentrated at their centers;

- there are no external nor internal forces acting on the two masses, but the gravitational force.
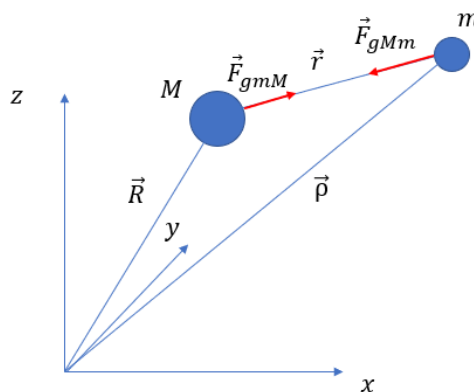
Figure 3.3: Two-body problem scheme.

It is possible to investigate the evolution of the position of the two bodies by introducing the second law of motion (or Newton's law), which states that a force acting on a mass produces an acceleration directly proportional to that force and inversely proportional to the body

mass:

$$\vec{F} = m\ddot{\vec{r}} \tag{3.3}$$

If we write an equilibrium equation for each mass and then divide by the same mass and sum each member of the equations, we will have:

$$\ddot{\vec{r}} = -\frac{G(M + m)}{r^3}\vec{r} \tag{3.4}$$

If the mass M is much greater than the mass m it is possible to make an approximation by considering (M+m) $\simeq$ M, so that we can write:

$$\ddot{\vec{r}} + \frac{\mu}{r^3}\vec{r} = 0 \tag{3.5}$$

where $\mu = Gm$ is the gravitational parameter, whose value is typical of the main body we are considering. It is worth reminding that the reference frame in which the equations above are written is an inertial one, that means it is still with respect to fixed stars.

Table 3.1: Values of μ for some celestial bodies

Celestial body	Gravitational parameter μ
Earth	$398\,629\,\text{Nm}^2/\text{kg}$
Moon	$4900\,\text{Nm}^2/\text{kg}$
Sun	$1.3275 \times 10^{11}\,\text{Nm}^2/\text{kg}$
Mars	$42\,839\,\text{Nm}^2/\text{kg}$

3.1.3   Constants of the motion

Before integrating the equation of motion, it is useful to manipulate it, in order to derive a series of useful scalar quantities, as their values can give important information about the properties of the orbit itself. The gravitational field generated by an M mass, as described by Newton in the 17th century, is a conservative field, which means that a body moving only under the influence of the M mass does not lose or gain mechanical energy, but it can only exchange one form of energy, called the "potential energy" with the other form of energy, called "kinetic energy". In the same way, it can be noticed that, as the gravitational force is always directed along the straight line connecting the two masses, it is possible to define a quantity, called angular momentum, that does not change when the the two masses interact or one orbit around the other. Starting from the equation of the two-body problem and then mathematically manipulating it, we obtain the expression of the mechanical energy that is, as already said, constant:

$$\mathcal{E} = \frac{v^2}{2} - \frac{\mu}{r} = constant \tag{3.6}$$

Working on the same equation, we can derive the expression of the angular momentum h that is, as already mentioned, constant in time:

$$\vec{h} = \vec{r} \times \vec{v} \tag{3.7}$$

Given that the angular momentum is the vector product of the radius and the velocity, we can state that it is perpendicular to both the aforementioned vectors and, consequentially, to the plane on which the two vectors lie. This also means that the velocity and the radius vectors of the mass orbiting around the other always lie on the same plane, determining a planar motion. It is important to clarify that both the mechanical energy and the angular momentum are calculated per unit of mass, so they are also called specific mechanical energy and specific angular momentum.

3.1.4 The trajectory equation

After obtaining the constant of motion it is worth, as to completely describe the trajectory of any mass orbiting the main mass M, deriving the trajectory equation. We start from the same point as we did to calculate the constants of motion, that is the equation of motion. After manipulating it and integrating both sides of it, we will obtain the following equation:

$$r = \frac{\frac{h^2}{\mu}}{1 + \frac{B}{\mu}cos\nu} \tag{3.8}$$

where the term B is the modulus of an integrative constant vector, introduced in the previous integration of the equation of motion, and it points toward the periapsis, which is the closest point to the focus point. Now it is useful to compare the form of this last equation to the general equation of a conic, written in polar coordinates with the origin located at a focus, and where the polar angle ν is the angle between the straight line passing through the point of the conic we are considering and the one passing through the periapsis. But before moving on, it is necessary to define what a conic is. A conic is defined as the curve of the intersection of a plane and a right circular cone. If the plane cuts across one nappe (half-cone), the section is an ellipse. A circle is just a special case of the ellipse where the plane is parallel to the base of the cone. If the plane is parallel to a line on the surface of the cone, the section is a parabola. If the plane cuts both nappes, the section is a hyperbola having two branches.
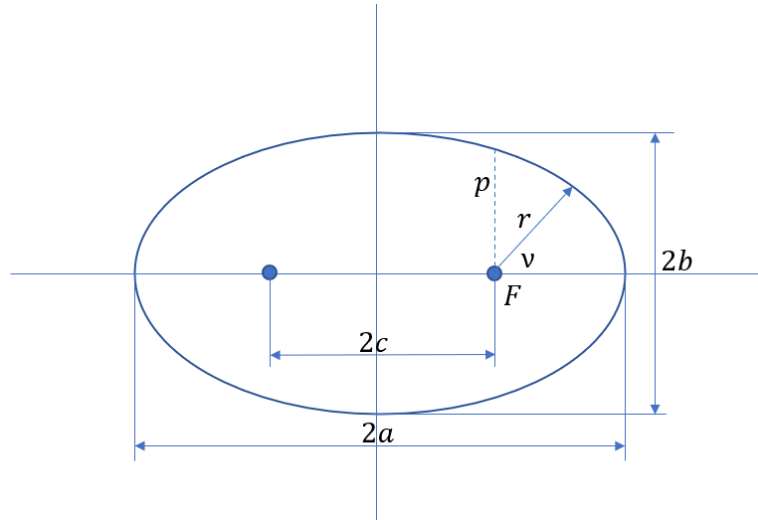
Figure 3.4: Representation of the ellipse.

Therefore, we can write:

$$r = \frac{p}{1 + e\cos\nu} \tag{3.9}$$

where the parameter p is called semilatus rectum and e is the eccentricity and it determines the type of conic section represented by the equation. It is clear that the two equations are formally identical, thus we can conclude that the trajectory followed by any mass orbiting the main mass M is a conic with the main mass M located in one of the foci, assuming the two-body problem's hypotheses. As mentioned above, depending on the value of the eccentricity e, we can have a circle, if $e = 0$, an ellipse if $0 < e < 1$, parabola if $e = 1$ and a hyperbola if $e > 1$. Therefore, we can describe, with just one equation, any type of trajectory a mass can follow, only by changing the value of e. Starting from the analogy between the two equations, we can also relate the semi-major axis, the eccentricity, and the semilatus rectum as follows:

$$e = \frac{c}{a} \tag{3.10}$$

and

$$p = a(1 - e^2) \tag{3.11}$$

with a that, as explained in the next pages, defines the orbit size. Two important points of the conic that are worth defining mathematically are the periapsis, which we already introduced before, and the apoapsis. They are defined, respectively, as the nearest and the farthest point from the focus, or alternatively, as the points where $\nu = 0\,\mathrm{deg}$ and $\nu = 180\,\mathrm{deg}$. Therefore, considering the equation of a conic defined previously, we can state that:

$$r_p = a(1 - e) \tag{3.12}$$

and

$$r_a = a(1 + e) \tag{3.13}$$

3.1.5 Relation between energy and geometry of an orbit

We've already shown how the angular momentum h does not change along the orbit. For the same reason, it remains constant in the two main points of the orbit we discussed before, the periapsis and the apoapsis. Therefore, we can write:

$$h = r_p v_p = r_a v_a \tag{3.14}$$

Moreover, we can express the mechanical energy of the orbit as:

$$\mathcal{E} = \frac{v^2}{2} - \frac{\mu}{r} = \frac{h^2}{2r_p} - \frac{\mu}{r_p} \tag{3.15}$$

but the radius of periapsis is:

$$r_p = a(1 - e) \tag{3.16}$$

and comparing the equation of a conic with the equation of the trajectory for the two-body problem, we can state:

$$h^2 = \mu a(1 - e^2) \tag{3.17}$$

and substituting in the expression of the specific mechanical energy, we obtain:

$$\mathcal{E} = -\frac{\mu}{2a} \tag{3.18}$$

which relates the specific mechanical energy itself with the semi-major axis of the orbit.

3.1.6 Classical orbital elements

Five independent quantities called "orbital elements" are sufficient to completely describe the size, shape and orientation of an orbit. A sixth element is required to fix the position of the satellite along the orbit at a particular given instant of time.
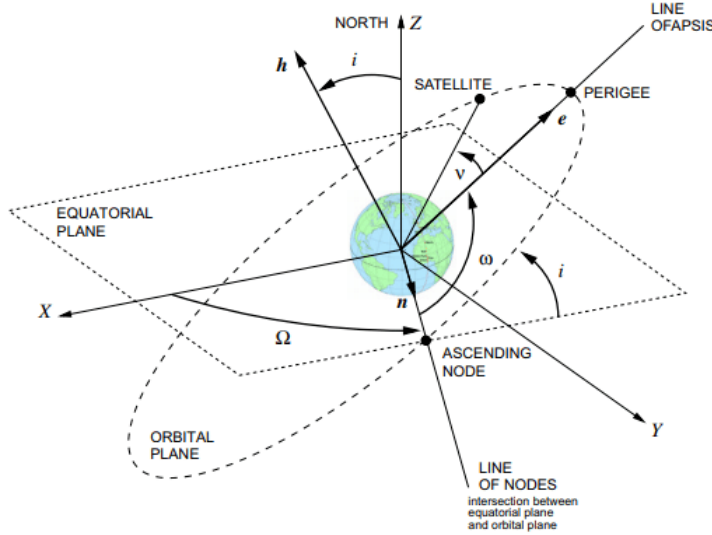
Figure 3.5: Classical orbital elements. [15]

The six classical orbital elements are defined as follows:

- Semi-major axis **a**: a constant defining the size of the orbit;

- Eccentricity **e**: that define the shape of the orbit;

- Inclination ι: defined as the angle between the angular momentum vector $(\vec{h})$ and the unit vector $\hat{K}$;

- Longitude of ascending node Ω: the angle, in the fundamental plane, between the $\hat{I}$ unit vector and the point where the satellite crosses through the fundamental plane in a northerly direction (ascending node) measured counterclockwise when viewed from the north side of the fundamental plane;

- Argumentum of periapsis ω: the angle, in the plane of the satellite's orbit , between the ascending node and the periapsis point, measured in the direction of the satellite's motion;

- True anomaly $\nu(t)$: defined as the angle between the radius of the orbiting mass at time t $(r(t))$ and the periapsis direction.

Alternatively, another parameter can replace the true anomaly, which is the *mean anomaly*, defined as:

$$M = t_{PK}\sqrt{\frac{\mu}{a^3}} \tag{3.19}$$

where t_{PK} is the elapsed time to go from the periapsis point to the k point.

A further parameter will be used in this thesis in order to identify the angular position of the periapis, that is the *longitude of periapsis*, indicated as Π and defined as the angle from $\hat{I}$ to periapsis measured eastward to the ascending node (if it exists) and then in the orbital plane, whose expression is:

$$\Pi = \Omega + \omega \tag{3.20}$$

3.1.7 The elliptical, circular and parabolic orbits

The orbits of all planets in the Solar System are ellipses, therefore it is useful to give more information about the elliptical orbit, as it was the starting point to calculate the parameters of any kind of orbit.

One of the properties of the ellipsis is that, for any given point the sum of the distances of that point from the two foci is constant, and equal to the semi-major axis, so:

$$r + r' = r_p + r_a = 2a \tag{3.21}$$

where it can be noticed we referred to the apoapsis and periapsis point as well. Given that $e = c/a$ where c is the semi-distance between the two foci, we can express the eccentricity as :

$$e = \frac{r_a - r_p}{r_a + r_p} \tag{3.22}$$

Another important aspect of the elliptical orbit is related to time, so to the period of the elliptical orbit itself. In fact, it is possible to rewrite the angular momentum as:

$$h = r^2 \frac{d\nu}{dt} \tag{3.23}$$

but, from elementary calculus we know that the differential element of area, dA, swept out by the radius vector as it moves through an angle $d\nu$, is:

$$dA = \frac{1}{2} r^2 d\nu \tag{3.24}$$

thus we can state that dA/dt is a constant quantity along the orbit, just like the second law of Kepler, not presented in this work, states, so we can substitute dA with the ellipsis area and dt with the period τ, obtaining the expression of the period of the elliptical orbit

$$T = 2\pi \sqrt{\frac{a^3}{\mu}} \tag{3.25}$$

As already mentioned, the circular orbit is a particular case of the elliptical orbit, where the distance between the two foci is equal to zero. This means also that if we substitute the semi-major axis, in all the previous formulas, with the radius r, which is constant, we can refer to the same expressions for the circular orbit as well.

If we want the elapsed time between two positions of the rotating mass on its orbit, knowing the angular position at the two instants of time, then it is necessary to make a geometrical evaluation on the ellipsis.
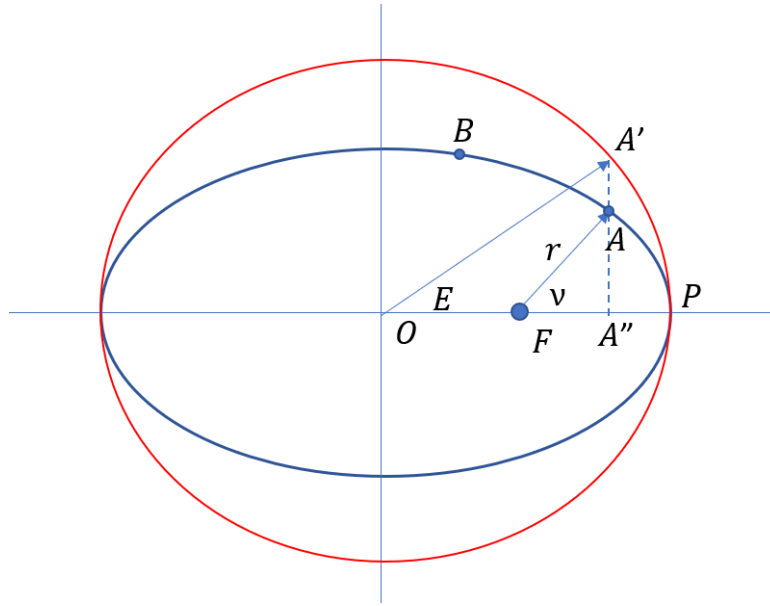
Figure 3.6: Direct time problem scheme.

If we consider an A point on the ellipsis and we project the point on a circumference of radius a, we define a A' point, which angular position with respect to the axes origin will be equal to the *eccentric anomaly* E. Therefore, we will refer to this angle to calculate the time t_{AtoB}, as the difference between the elapsed time to go from periapsis to B and the elapsed time to go from periapsis to A. After geometrical observations and calculations we get to write:

$$t_{AtoB} = t_{PtoB} - t_{PtoA} = \sqrt{\frac{a^3}{\mu}}[(E_B - esinE_B) - (E_A - esinE_A)] \tag{3.26}$$

The elliptic orbit is not the only type of trajectory an orbiting mass can follow as, in general, the trajectory is a conic, then circular, hyperbolic, and parabolic orbits are possible as well. The parabolic orbit, in particular, is an open orbit, together with the hyperbolic orbit, and it's fundamental in order to escape the gravity of a celestial body. In fact, any object escaping a planet will follow either a parabolic or a hyperbolic trajectory, depending on its energy at an infinite distance with respect to the main mass it is escaping. In fact, if the escaping mass comes to an infinite distance with mechanical specific energy equal to zero, the trajectory will be a parabola, while, if the energy is not zero, the body will follow a hyperbolic trajectory.

It is possible to calculate the escape velocity, assuming that the escape trajectory is a parabola, starting from the expression of the mechanical energy:

$$\mathcal{E} = \frac{v_{esc}^2}{2} - \frac{\mu}{r} = \frac{v_\infty^2}{2} - \frac{\mu}{r_\infty} = 0 \tag{3.27}$$

At last we get:

$$v_{esc} = \sqrt{\frac{2\mu}{r}} \tag{3.28}$$

where r is the radius, from the planet's center, when the spacecraft is at the beginning of the escape maneuver.

3.1.8 Interplanetary trajectories maneuvers

In this section, the fundamental maneuvers occurring during an interplanetary mission will be presented only with respect to the heliocentric frame of reference, as the escape trajectory from the Earth and the arrival to the target asteroid are not object of this thesis.

Before introducing the problem of interplanetary trajectories, even though it is not part of this thesis, it is useful to introduce the method of patched conics together with the concept of the sphere of influence of a planet.

The *sphere of influence* of a planet is defined as that region of space, surrounding the planet itself, where the gravitational effects on a mass that is located in it, is predominant with respect to the effects of all other planets. The radius of this sphere can be calculated with the following formula:

$$r_{SOI,planet} = \left(\frac{m_{planet}}{M_{Sun}} \right)^{2/5} r_{planet} \tag{3.29}$$

where r_{planet} is the mean distance of the planet from the Sun.

The *patched-conic approximation* is based on the idea that, during an interplanetary transfer, we can assume the trajectory of the spacecraft is composed of three parts: the first part is the geocentric phase, where the spacecraft is influenced only by Earth gravity. After escaping the Earth's gravity, it will be effected only by the Sun's gravity and, at the arrival to the target, the only gravitational effects will be caused by the target celestial body. As already specified, in this thesis, only the heliocentric phase will be analyzed.

The fundamental transfer maneuver between two orbits is the so-called **Hohmann transfer**, taking its name from the German engineer who first theorized it. The Hohmann transfer is the one that guarantees the least consumption in terms of ΔV and assumes the initial and final orbit to have different radii and to be circular and coplanar. This is a strong simplification, as most of the orbits of either planets and asteroids are neither circular nor coplanar with one another, as they have eccentricities $e \neq 0$ and different ιs.
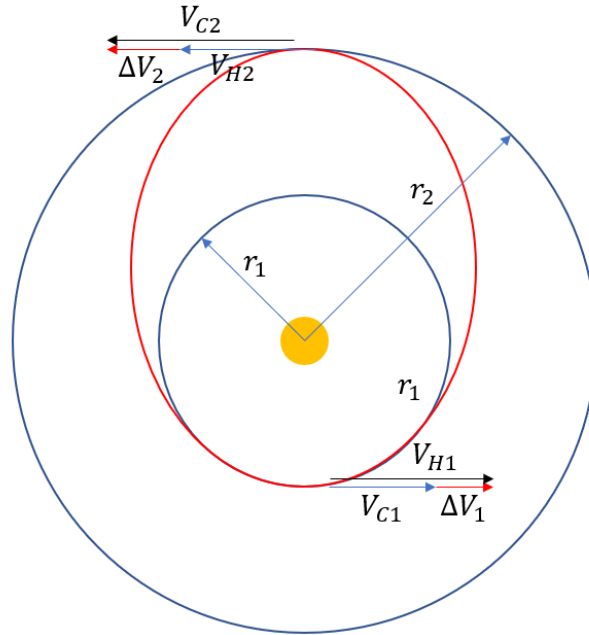
Figure 3.7: Scheme of Hohmann transfer.

The transfer orbit is a semi-elliptical orbit, whose periapsis is common to the lower orbit and apoapsis common to the higher orbit. The maneuver is performed with two impulses: the first one is supposed to insert the spacecraft into the transfer orbit, while the second one circularizes the transfer orbit itself, thus leading the spacecraft to the target orbit. The two thrust firings will be applied parallel to the velocity in both cases, which, as explained in the next chapter, avoids losses due to misalignment of the thrust. The semi-major axis of the transfer orbit a_t is defined as:

$$a_t = \frac{r_1 + r_2}{2} \tag{3.30}$$

where r_1 and r_2 indicate the radii of the initial orbit and final orbit, respectively. The cost of the whole maneuver is given by the sum of the costs of the two impulses ΔVs. Thus we can state:

$$\Delta V_{tot} = \Delta V_1 + \Delta V_2 \tag{3.31}$$

with

$$\Delta V_1 = \sqrt{\frac{\mu}{r_1} \left(\frac{2r_2}{r_1 + r_2} - 1 \right)} \tag{3.32}$$

$$\Delta V_2 = \sqrt{\frac{\mu}{r_2} \left(1 - \frac{2r_1}{r_1 + r_2} \right)} \tag{3.33}$$

The duration of the Hohmann transfer can be calculated by reminding the formula of an orbit period and noticing that it is a semi-elliptical orbit, therefore:

$$T_H = \pi \sqrt{\frac{a_t^3}{\mu}} \tag{3.34}$$

Anyway, the Hohmann transfer is only one of the possible maneuvers to move from one orbit to another one. In fact, other trajectories are possible, such as a parabolic transfer or a hyperbolic transfer. Obviously, the thrust needed to insert the spacecraft into a parabolic transfer is higher than the one needed in the case of Hohmann transfer and if we consider transferring on a hyperbolic trajectory, the cost in terms of ΔV is even higher than the parabola. The transfer duration, on the other hand, decreases if we go from a Hohmann transfer to a parabolic one until the shortest duration of the hyperbolic one.

Two more maneuvers that are worth being introduced are performed with just one impulse, which are the absides line rotation and the simple plane change. The first one, as suggested by its name, is needed to rotate the line of absides, thus changing the positions of periapsis and apoapsis.
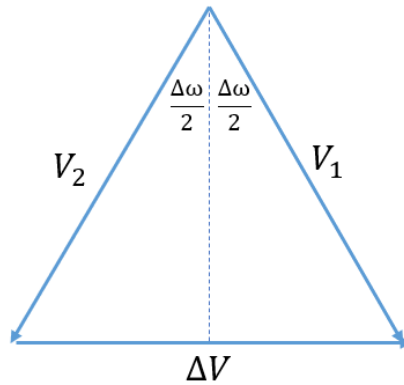
Figure 3.8: Geometrical representation of V_1, V_2 and ΔV vectors in a maneuver of absides rotation.

The cost of this maneuver is:

$$\Delta V = 2\frac{\mu}{h}e|sin\left(\frac{\Delta\omega}{2}\right)| \tag{3.35}$$

with h specific angular momentum of the orbit, and $\Delta\omega$ the variation of the argumentum of periapsis.

The simple plane change is needed to change the orbit inclination, and, as shown in the figure below, the cost of this maneuver (ΔV) can be calculated as:
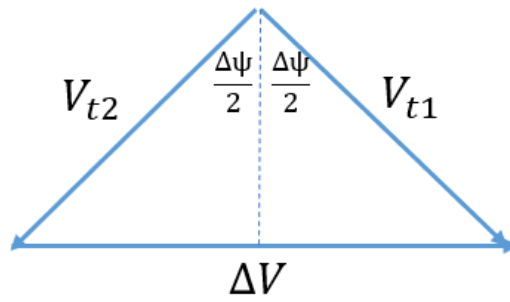
Figure 3.9: Geometrical representation of V_1, V_2 and ΔV vectors in a maneuver of inclination change.

$$\Delta V = 2V_t e|sin\left(\frac{\Delta \psi}{2}\right)| \tag{3.36}$$

with V_t being the tangential component of the velocity vector and $\Delta \psi$ being the difference between final and initial azimuth angles.

The last two important quantities to properly define the problem of interplanetary missions are the **phase angle** γ and the **sinodic period** τ_s. The phase angle is defined as the angle between the Earth and the planet (or the asteroid) on which we want to get, at the beginning of the missions. Therefore, the spacecraft will leave the Earth's sphere of influence and begin the heliocentric phase when the angular distance between the Earth and the final destination will be exactly equal to the phase angle, or γ angle.
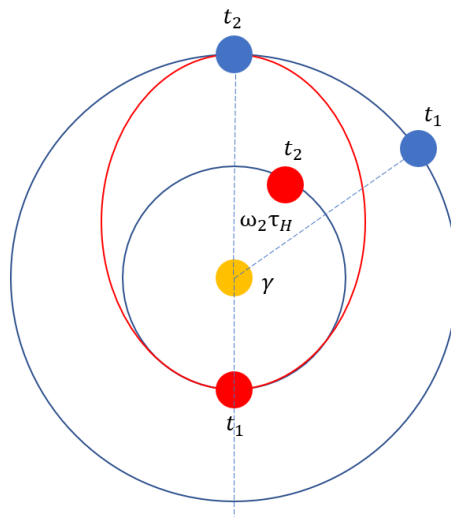
Figure 3.10: Representation of phasing problem.

This instant of time is also called **launch window**. The equation used to find the value of γ is:

$$\gamma + \omega_2\tau_H = \pi \tag{3.37}$$

where ω_2 is the angular velocity of the destination planet or asteroid and τ_H is the duration of the Hohmann transfer. If we miss the launch window, we have to wait a period of time called **sinodic period**, calculated as:

$$\tau_s = \frac{2\pi}{|\omega_1 - \omega_2|} \tag{3.38}$$

where ω_1 is the angular velocity of the starting planet.

3.2 Fundamentals of space propulsion

The second main branch of physics involved in the development of this work is space propulsion, therefore the basic concepts are summarized down below.[16] [17] [18]

In space propulsion, the thrust is produced by taking advantage of the principle of action and reaction. Let's start by considering a mass m, moving forward at a velocity V, as shown in the figure below. After a time dt, the original mass loses an elementary amount of mass dm_p that will move in the opposite direction at an absolute velocity $c - V$, where c is the velocity of ejection of the mass dm_p, with respect to the mass m, while the original mass, whose value is now $m - dm_p$, moves at a velocity equal to $V + dV$, thus increasing its velocity.
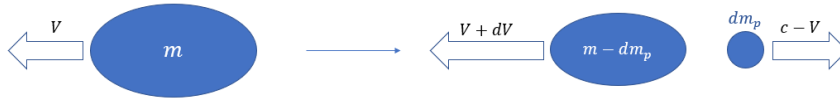
Figure 3.11: One-dimensional representation of thrust generation.

The one-dimensional physical system we are considering is an isolated system, therefore, the momentum is conserved. Thus, we can write:

$$mV = (m - dm_p)(V + dV) - dm_p(c - V)$$

$$mV = mV - dm_pV + mdV - dm_p dV + dm_pV - dm_p c$$

and, if we neglect the higher order terms, we get to:

$$mdV = dm_p c$$

This result was obtained for the ejection of a discrete mass, if we consider a continuous flow of mass we can write:

$$dm_p = \dot{m}_p dt$$

$$dV = \frac{dV}{dt} dt$$

and, substituting in the former equation, we get:

$$m\frac{dV}{dt} = \dot{m}_p c$$

It can be noticed that this last equation is formally similar to Newton's law, but in this case, we have a variable mass. The rate of mass change is equal to:

$$\frac{dm}{dt} = -\dot{m}_p$$

and the mass m itself undergoes a thrust, with the same direction as the vector c, but of opposite sign. The thrust produced by the ejection of the continuous mass flow $\dot{m}_p$ is equal to:

$$T = \dot{m}_p c \tag{3.39}$$

and we call **c** the exhaust velocity.

Moreover, it is useful to calculate the value of the power needed to eject the propellant with an exhaust velocity equal to c, thus we have:

$$P_T = \frac{1}{2}\dot{m}_p c^2$$

or alternatively

$$P_T = \frac{Tc}{2} \tag{3.40}$$

There are two more physical quantities that are useful to describe the performances of a propulsion system, that are the **total impulse** and the **specific impulse**. With the total impulse, we take into account the cumulative effects the thrust produces, so its mathematical expression will be:

$$I_{tot} = \int_{t_0}^{t_f} T(t)dt \tag{3.41}$$

and, if the thrust is constant, we can simplify the former expression as follows:

$$I_{tot} = T\Delta t \tag{3.42}$$

The second physical quantity we've just mentioned is the specific impulse, whose definition is:

$$I_{sp} = \frac{I_{tot}}{m_p g_0} \tag{3.43}$$

this last expression is considerably more important than the other one, as it gives information about how well we are using the propellant. In fact if we look at the numerator, we can notice

that it can be seen as a useful effect, while the denominator is the cost of the thrust. In fact, m_p is the mass of propellant we spend to generate the thrust, while g_0 is the gravity acceleration on Earth, thus its expression indicates the weight of propellant spent during a period of time $t_f - t_0$. So the specific impulse can be seen as a sort of thrust efficiency and, if the thrust is constant, it can be simplified as:

$$I_{sp} = \frac{c}{g_0} \tag{3.44}$$

The specific impulse can be also seen as a characteristic time: in fact, it indicates the period of time when a certain mass of propellant can guarantee a thrust equal to its weight at sea level on Earth.

In this work, we will consider a low level of thrust and long-term missions, therefore, the specific impulse will be high. The final aim of a space propulsive system is to change the velocity of the spacecraft itself, so it is convenient to calculate the change of velocity (ΔV) with respect to the spent propellant or, alternatively, as it is more common, to the mass ratio $(\frac{m_f}{m_0})$. We can state that, if we assume that thrust is parallel to the velocity, the ideal ΔV can be obtained by integrating the acceleration due to the thrust T between an initial and a final time, in formula:

$$\Delta V = \int_{t_0}^{t_f} \frac{T}{m} dt$$

and reminding that $T = \dot{m}_p c$, it is possible to write the last expression as:

$$\Delta V = \int_{t_0}^{t_f} \frac{\dot{m}_p c}{m} dt$$

and given that $\dot{m}_p = -\frac{dm}{dt}$, we finally obtain:

$$\Delta V = -c \int_{m_0}^{m_f} \frac{dm}{m}$$

and integrating:

$$\Delta V = c \ln \frac{m_0}{m_f} \tag{3.45}$$

or alternatively:

$$\frac{m_f}{m_0} = e^{\frac{-\Delta V}{c}} \tag{3.46}$$

This last expression is also called the *Tsiolkovsky equation* and it is maybe the most important equation in space propulsion as it relates the useful effect (ΔV) with the mass ratio. The following table underlines the effects of velocity variation and the exhaust velocities on the mass ratio. In fact the lower $\Delta V/c$ is, the higher the mass ratio will be, thus decreasing the quantity of fuel carried by the spacecraft thus increasing the payload mass. This explains the

importance of limiting the ΔV of a mission by optimizing the trajectory, also considering types of propulsion whose typical exhaust velocities are high.

Table 3.2: Values of mass ratios in relation to $\Delta V/c$ values. [18]

$\Delta V/c$	m_f/m_0
5	0.0067
2	0.135
1	0.368
0.5	0.606
0.2	0.819
0.1	0.905

It is also interesting to investigate the velocity variation from the point of view of the spacecraft, but now we will take into account the losses always occurring in space propulsion, thus evaluating their magnitude and how to limit them.
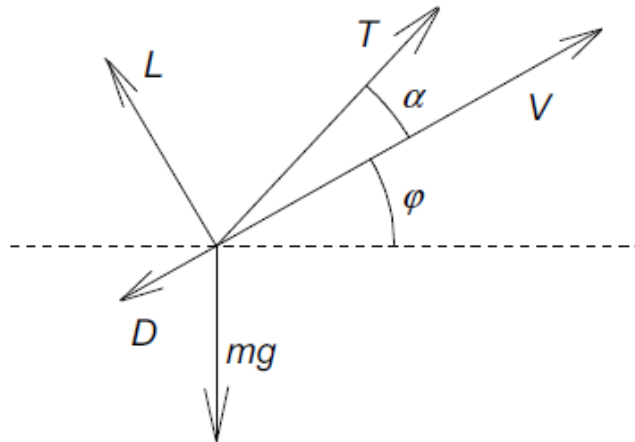
Figure 3.12: Free body diagram of a spacecraft during atmospheric flight. [18]

We will consider four contribution to the force applied on the spacecraft itself, therefore:

$$m\frac{d\vec{V}}{dt} = \vec{T} + m\vec{g} + \vec{D} + \vec{L}$$

where $\vec{T}$ is the thrust vector, $\vec{g}$ is the gravity acceleration of the celestial body around which the spacecraft is orbiting, and $\vec{D}$ and $\vec{L}$ are the drug and the lift applied to the spacecraft during the atmospheric phase of flight, which will be not considered in this work. Rearranging the terms of the equation and considering scalar quantities, and neglecting the lift term:

$$\frac{dV}{dt} = \frac{T}{m}cos\alpha - \frac{D}{m} - gsin\varphi =$$

$$= \frac{T}{m} - \frac{T}{m}(1 - cos\alpha) - \frac{D}{m} - gsin\varphi$$

and integrating between the initial and final instant of times:

$$V_f - V_0 = \int_{t_0}^{t_f} \frac{T}{m}dt - \int_{t_0}^{t_f} (1 - cos\alpha)dt - \int_{t_0}^{t_f} \frac{D}{m}dt - \int_{t_0}^{t_f} gsin\varphi dt \qquad (3.47)$$

we get to the final expression:

$$V_f - V_0 = \Delta V - losses \qquad (3.48)$$

The losses just mentioned are due to three main contributions:

- **misalignment losses**: $\int_{t_0}^{t_f}(1 - cos\alpha)dt$ due to the misalignment between the thrust and the velocity vectors, which can be avoided by applying the thrust always parallel to the velocity;

- **drag losses**: $\int_{t_0}^{t_f} \frac{D}{m}dt$ due to the friction with the atmosphere; we will neglect this term in our calculations;

- **gravity losses**: which are present if the spacecraft's velocity vector is not perpendicular to the local gravity vector, then they are equal to $\int_{t_0}^{t_f} gsin\varphi dt$, where φ is the flight path angle, that is the angle between the velocity vector the the local horizon.

Focusing specifically on space propulsion, it is possible to distinguish two main types of propulsion, that are:

- **Chemical propulsion**: where propellants in the chamber react, producing hot gases that, conducted in a nozzle, expand, producing an acceleration and thus a thrust;

- **Electric propulsion**: where the source of energy is separated from the propellant and does not depend on it.

For electric propulsion, as the source of energy is separated from the propellant, it is necessary to supply energy or power, and because of it, a power generator is needed. Therefore, we have several types of generator, such as:

- Solar panels: that convert solar power into electric power, supplying it to the engine;

- Energy by radioisotopes or nuclear fission reactors: that supply a high amount of thermal energy, that has to be converted into electric energy.

As already mentioned, the typical specific impulses for electric propulsion are high, therefore it is necessary to guarantee an adequate exhaust velocity value, which is nearly 10 km/s for electric propulsion. To this aim, we have to change the employed type of propulsion as the simple heating of a propellant stream by chemical reaction or a solid element heat transfer, typical of chemical propulsion, would not be appropriate. In fact, the heating would have to be supplied by an external agent that has considerably higher heat release capability, and in addition, the propellant gas so heated should be kept away from the material walls of the

heating chamber and nozzle. Such a sophisticated heater would not be able to provide the upper range of desired exhausted velocities, therefore, we need to directly apply body forces to the propellant stream. This process is most reasonably accomplished by electrical means. We can thus characterize electric propulsion as the acceleration of gases for propulsion by electrical heating and/or by electric and magnetic body forces. We can also divide it into three distinct concepts:

- **electrothermal propulsion**, where the propellant gas is heated electrically, then expanded in a nozzle;

- **electrostatic propulsion**, where the propellant is accelerated by direct application of electric body forces to ionized particles;

- **electromagnetic propulsion**, where an ionized propellant stream is accelerated by interactions of external and internal magnetic fields with electric currents driven through the stream.

It is important to notice that there is a power supply penalty in electric propulsion, as the power sources have to be carried with the payload in the spacecraft. In particular, its mass can be assumed to be directly proportional to the exerted power, thus we write:

$$m_{source} = \alpha P = \frac{\alpha T c}{2\eta} = \frac{\alpha g_0 T I_{sp}}{2\eta} \tag{3.49}$$

The last but not least aspect to be underlined is that, normally, low thrust engines, like the one we will consider in this work exert a thrust that is not adjustable, therefore the modulus of the thrust itself will be either T_{max} or 0, thus on or off. The definition of thrust level (T_{max} or 0) will be performed exploiting a switching function, defined in the next chapters, which value will determine the engine firing intervals.

Chapter 4

Mathematical model

The aim of the whole work of this thesis is the optimization of interplanetary trajectories which has been a key point since the beginning of the space missions' era. For this reason, in the following sections, the problem of the optimization will be introduced together with one of the possible approaches to solve it, the indirect optimization, that has been adopted to calculate the most significant parameters of the missions.

4.1 Indirect optimization of space trajectories

The problem of optimization consists in finding a proper control law that maximizes or minimizes a specific performance index. In a space mission fuel mass has crucial importance to make the mission itself possible, in terms of technologies and costs, so that the fuel consumption must be the lowest possible or, conversely, the final mass of the spacecraft must be the highest possible, once the initial is fixed. The analytic solution to this problem is possible only for a few simple cases, that are not of interest to this thesis, as the simplifications needed to make it solvable are so strong that it has a weak physical meaning. Therefore, the problem has to be solved with numerical methods among which indirect optimization is a convenient one. In fact, they are characterized by high numerical precision and meaningful theoretical content. Moreover, the low number of parameters and the short time of calculation make it suitable for the aim of this thesis, even though it has difficulties of convergence and weak robustness as well.

4.2 Theory of optimal control

In the following section the theory of optimal control, based on principles of variational calculus, will be exposed.

The generic system, on which the theory of optimal control is applied, is defined by a vector of state variables $\mathbf{x}$ and the differential equations which describe its evolution between the initial and the final instant of time (external boundaries) are functions of $\mathbf{x}$, of controls vector $\mathbf{u}$ and of the independent variable of time $\mathbf{t}$. We can formally express the system as follows:

$$\frac{d\mathbf{x}}{dt} = \boldsymbol{f}(\mathbf{x}, \mathbf{u}, t) \tag{4.1}$$

In our case, it is convenient to divide the trajectory into a series of n sub-intervals, or arches, in which the state variables have to be continuous. The j-th interval starts at the time $t_{(j-1)+}$ and ends at the time $t_{(j)-}$, where the signs $+$ and $-$ indicate, respectively, the values assumed by the variable right before and right after the point we are considering. The state variables, therefore, will assume the values indicated by $\mathbf{x}_{(j-1)+}$ and $\mathbf{x}_{(j)-}$ in the same instant of time. This formalism allows to handle eventual discontinuity of variables and time, such as mass or velocity discontinuity after an impulsive maneuver, in the internal boundaries, that are the joint points of each arch and, in addition, it is possible to define a different value of the second member of the former equation for each considered sub-interval.

The boundary conditions, which are imposed both on the internal and on the external boundaries, are mixed conditions, and they can be mathematically written as follows.

$$\chi(\mathbf{x}_{(j-1)+}, \mathbf{x}_{j-}, t_{(j-1)+}, t_{j-}) = 0 \tag{4.2}$$

with $j = 1, ..., n$.

The problem of the research of the optimum can be formalized as the research of the extremal values, so maximum or minimum, of a functional we can generally express as:

$$J = \varphi(\mathbf{x}_{(j-1)+}, \mathbf{x}_{j-}, t_{(j-1)+}, t_{j-}) + \sum_j \int_{t_{(j-1)+}}^{t_{(j)-}} \Phi(\mathbf{x}(t), \mathbf{u}(t), t) dt \tag{4.3}$$

It is possible to notice how the functional is the sum of two terms, the function φ which depends on the values assumed by time and variables at the internal and external boundaries and on the integral, extended to the whole trajectory, of the function Φ whose value, on its hand, depends on time and variables on all the points of the trajectory. From this formalism, we can always introduce new auxiliary variables to rewrite the problem in the case $\varphi = 0$, which corresponds to the Lagrange formulation, or $\Phi = 0$, that is the Meyer formulation.

Getting back to the definition of functional J, it is possible to rewrite it, introducing the Lagrange multipliers, which are constant associated to the boundary condition and indicated as μ, and the variables λ, also called adjoint variables, which are associated to the state equation. Thus, we write:

$$J^* = \varphi + \mu^T \chi + \sum_j \int_{t_{(j-1)+}}^{t_{(j)-}} (\Phi + \lambda^T(f - \dot{x})) dt$$

with $j = 1, ..., n$.

As it is possible to notice, the two functionals depend on time t, on variables x, on the derivative in time of variables $\dot{x}$ or, more specifically, on the values that time and variables assume at the extremes of each arch, and on input vector u. The two functionals J and J^* coincide if both boundary conditions and state equation are satisfied, as well as their extremal values. If we integrate by parts, in order to eliminate the dependency on state variables' derivatives, we get:

$$J^* = \varphi + \mu^T \chi + \sum_j (\lambda_{(j-1)+}^T x_{(j-1)+} - \lambda_{j-}^T x_{j-}) + \sum_j \int_{t_{(j-1)+}}^{t_{j-}} (\Phi + \lambda^T f - \dot{\lambda}^T x) dt \tag{4.4}$$

$j = 1, ..., n.$

and, differentiating, we finally get the first variation of the functional δJ^* itself:

$$\delta J^* = \left(- H_{(j-1)+} + \frac{\partial \varphi}{\partial t_{(j-1)+}} + \mu^T \frac{\partial \chi}{\partial t_{(j-1)+}} \right) \delta t_{(j-1)+} +$$

$$+ \left(H_{j-} + \frac{\partial \varphi}{\partial t_{j-}} + \mu^T \frac{\partial \chi}{\partial t_{j-}} \right) \delta t_{j-} +$$

$$+ \left(\lambda^T{}_{(j-1)+} + \frac{\partial \varphi}{\partial x_{(j-1)+}} + \mu^T \left[\frac{\partial \chi}{\partial x_{(j-1)+}} \right] \right) \delta x_{(j-1)+} +$$

$$+ \left(- \lambda^T{}_{j-} + \frac{\partial \varphi}{\partial x_{j-}} + \mu^T \left[\frac{\partial \chi}{\partial x_{j-}} \right] \right) \delta x_{j-} +$$

$$+ \sum_j \int_{t_{(j-1)+}}^{t_{j-}} \left(\left(\frac{\partial H}{\partial x} + \dot{\lambda}^T \right) \delta x + \frac{\partial H}{\partial u} \delta u \right) dt \qquad (4.5)$$

with j=1,...,n.

It can be notice as, in the previous equation, the Hamiltonian H has been introduced, which is defined as:

$$H = \Phi + \lambda^T f \qquad (4.6)$$

The optimum condition implies the stationarity of the functional J^*, therefore its first derivative has to be equal to zero for any value assumed by the variations $\delta x, \delta u, \delta x_{(j-1)+}, \delta x_{j-}, \delta t_{(j-1)+}$ and δt_{j-} compatible with the differential equations and the boundary conditions. Moreover, by properly choosing the values of the adjoint variables, it is possible to nullify all the coefficients of the variations appearing in the equation above at the same time, thus satisfying the condition of stationarity of the functional, expressed by $\delta J^* = 0$.

So if we nullify the coefficients of δx and δu appearing in the integrals in the equation above for each point of the trajectory, we will get, for the state vector:

$$\frac{d\lambda}{dt} = - \left(\frac{\partial H}{\partial x} \right)^T \qquad (4.7)$$

and, for the input vector:

$$\left(\frac{\partial H}{\partial u} \right)^T = 0 \qquad (4.8)$$

It is important to specify that the condition of stationarity of the functional does not discriminate the value of a maximum and of a minimum of the functional itself. If a constraint condition has to be imposed, that is, if the solution has to belong to a domain of admissibility, the optimal values of the control in each point of the trajectory is the one that, belonging to the

domain of admissibility, makes maximum, or minimum, the Hamiltonian in the same points. It is important to notice that the constraints we are considering, are supposed to be explicit and constant along the trajectory itself.

In order to further clarify this latest concept, we can state that:

- the optimal value of control u is the one resulting from the equation above, if it belongs to the admissibility domain, therefore the constraint does not affect the solution in that point (control locally not constrained);

- if the optimum control does not belong to the domain of admissibility, then the optimum control value will be equal to the extreme value of the domain itself, maximum or minimum (control locally constrained).

We have a particular case, when the Hamiltonian is linear with respect to one of the controls subject to the constraints, as in the equation reported above, the control input does not explicitly appear therefore, it cannot be determined. In this case, we can have two more possible options:

- if, in the equation, the coefficient of the aforementioned control is not equal to zero, then H will be maximized for the maximum value of the control input, if the coefficient is positive, or for the minimum value, if the coefficient is negative (bang-bang control), in accordance with the Principle of Maximum by Pontryagin;

- if, in the equation, the coefficient of the aforementioned control is identically equal to zero during a finite arch of time, also called singular arch, then we will impose all the successive coefficient derivatives to be null with respect to time, until, in one of these, the control will appear explicitly. The optimal control is determined by nullifying this last derivative. The order of this last derivative is always even and the order of the singular arch will be half of the derivative order.

Now, we need more boundary conditions, as to impose them on each of the extremes of the arches. So, if we refer to the j-th bound, we can apply the boundary conditions we already introduced, by considering it as the final extreme of the $(j-1)$-th interval or as the initial extreme of the j-th interval. If we nullify the coefficients of the differentials δx_{j-}, δx_{j+}, δt_{j-}, δt_{j+}, we will get:

$$-\lambda^T{}_{j-} + \frac{\partial \varphi}{\partial x_{j-}} + \mu^T \left[\frac{\partial \chi}{\partial x_{j-}}\right] = 0 \tag{4.9}$$

with $j = 1, ..., n$

$$-\lambda^T{}_{j+} + \frac{\partial \varphi}{\partial x_{j+}} + \mu^T \left[\frac{\partial \chi}{\partial x_{j+}}\right] = 0 \tag{4.10}$$

with $j = 0, ..., n-1$

$$H_{j-} + \frac{\partial \varphi}{\partial t_{j-}} + \mu^T \frac{\partial \chi}{\partial t_{j-}} = 0 \tag{4.11}$$

with $j = 1, ..., n$

$$-H_{j+} + \frac{\partial \varphi}{\partial t_{j+}} + \mu^T \frac{\partial \chi}{\partial t_{j+}} = 0 \qquad (4.12)$$

with $j = 0, ..., n-1$

where, analogously to the previous case, the subscripts $+$ and $-$ indicate the values right after and before the point j. It is important to notice that the formalism $j - 1$ does not make sense on the first interval, and so does $j + 1$ on the last one.

Moreover, if we eliminate the constants μ from the first and last equations, we will get the boundary condition written as:

$$\sigma(x_{(j-1)+}, x_{j-}, \lambda_{(j-1)+}, \lambda_{j-}, t_{(j-1)+}, t_{j-}) = 0 \qquad (4.13)$$

which completes the set of differential equations describing the mathematical problem. It is interesting to notice that, given a set of variables collected in the state vector x subject to a set of boundary conditions, the first two previous equations supply the corresponding optimum condition for the adjoint variables λ_x, in particular:

- if the state variable is explicitly fixed at the initial or final time, which means that the vector containing the imposed condition includes the equation $x_0 - a = 0$, with a fixed value of a, then there is no constraint on the corresponding adjoint variable λ_{x0}, which is free;

- if the initial (or final) value of the state variable x_0 does not appear either in the boundary condition or in the function φ, then the corresponding adjoint variable is null in the initial (or final) instant of time ($\lambda_{x0} = 0$);

- if a state variable is continuous but not fixed at an internal point i, hence the system χ contains the equation $x_{j+} = x_{j-}$, then the corresponding adjoint variable is continuous as well ($\lambda_{j+} = \lambda_{j-}$);

- if a state variable is continuous and explicitly assigned at an internal boundary, the system χ contains the equation $x_{j+} = x_{j-} = a$, then the corresponding adjoint variable has a free discontinuity, which means that the value of $\lambda_{x_{j+}}$ is independent of $\lambda_{x_{j-}}$ and it is determined by an optimization procedure.

In addition, if the Hamiltonian does not explicitly depends on time, the last two equations reported above can supply further boundary conditions, so that:

- if the initial time t_0 or the final time t_f does not appear either in the boundary conditions χ, or in the function φ, the Hamiltonian is null at the initial time and at the final time, respectively;

- if the intermediate time t_j does not explicitly appear in the expression of the function φ, so the only condition in which it is involved is the continuity condition at the internal boundaries ($t_{j+} = t_{j-}$), then the Hamiltonian is continuous in j, thus $H_{j+} = H_{j-}$;

- if time t_j is explicitly assigned, which means that in χ we have the equations $t_{j+} = t_{j-} = a$, the Hamiltonian has a free discontinuity in that point.

Chapter 5

Problem statement

In this chapter, the equations solved to get the final results will be introduced and discussed. The vector form of the equations has been formulated by projecting the equations themselves in an appropriate frame of reference, therefore we chose an inertial reference of frame as it is more convenient for the absence of drag and Coriolis accelerations, which would lead to a more complex system of equations, and for the correspondence existing between the adjoint variables of the components of velocity and the primer vector components, in the inertial frame. Therefore, we will refer to an inertial reference of frame fixed on the Sun, also called **heliocentric frame of reference**.
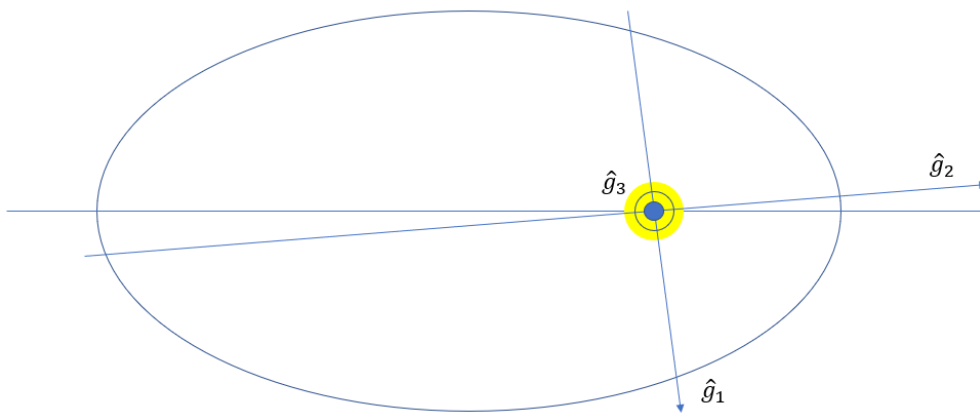
Figure 5.1: Heliocentric frame of reference.

The heliocentric frame of reference is characterized by having:

- origin fixed on the center of the Sun;

- the direction of x-axis (also defined as $\hat{g}_1$) defined by the intersection of the terrestrial equatorial plane and the ecliptic plane at the vernal equinox (on the 21st of March); the axis points toward the constellation of Aries;

- the z-axis (also defined as $\hat{g}_3$) perpendicular to the ecliptic plane, pointing toward the hemisphere containing Polaris;

- the y-axis (also defined as $\hat{g}_2$) completes the right-handed tern; it is important to notice that, even though the perihelion direction and the $\hat{g}_2$ direction are very close, they do not coincide.

Referring to this frame of reference, spherical coordinates will be adopted: the position of the spacecraft is described by the radius r, the longitude ϑ, and by the latitude ϕ, while the components of the velocity of the spacecraft by the radial component u zenith-pointing, the East-pointing component v and the north-pointing component w in a local frame of reference (ZEN), which means that this last frame is centered on the spacecraft itself and moves with it.
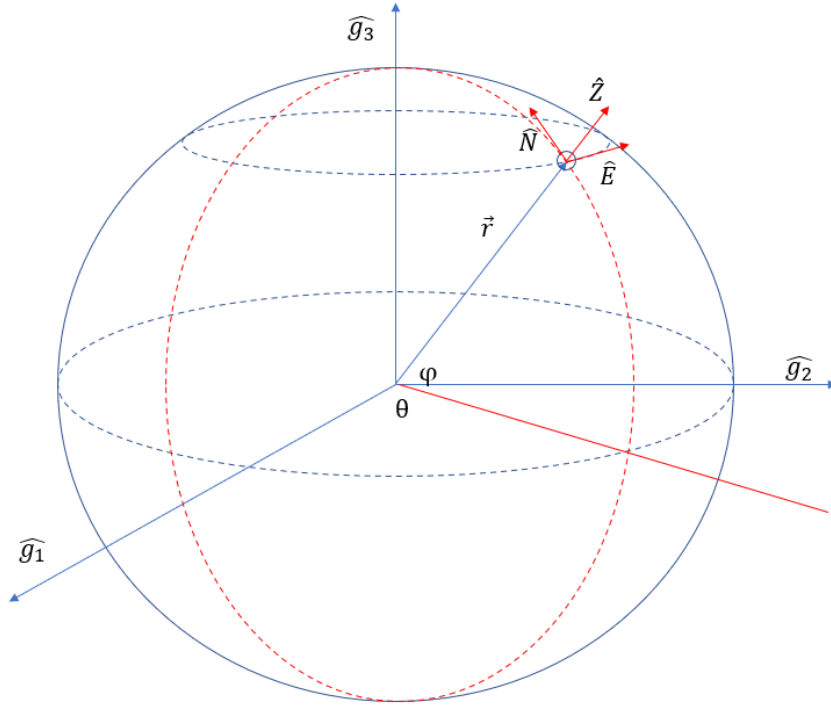
Figure 5.2: Representation of spherical coordinates.

The choice of projecting the components of the velocity on a local frame, instead of an axis that is parallel to the $\vec{V}$, is convenient as to have an easier relation between the absolute and the relative velocity.

Thus, projecting the equation on the aforementioned frame of reference, we get[19]:

$$\frac{dr}{dt} = u \tag{5.1}$$

$$\frac{d\vartheta}{dt} = \frac{v}{r cos\phi} \tag{5.2}$$

$$\frac{d\phi}{dt} = \frac{w}{r} \tag{5.3}$$

$$\frac{du}{dt} = -\frac{1}{r^2} + \frac{v^2}{r} + \frac{w^2}{r} + \frac{T}{m}sin\alpha \tag{5.4}$$

$$\frac{dv}{dt} = -\frac{uv}{r} + \frac{vw}{r}tan\phi + \frac{T}{m}cos\alpha cos\beta \tag{5.5}$$

$$\frac{dw}{dt} = -\frac{uw}{r} - \frac{v^2}{r}tan\phi + \frac{T}{m}cos\alpha sin\beta \tag{5.6}$$

$$\frac{dm}{dt} = -\frac{T}{c} \tag{5.7}$$

where γ and ψ are, respectively, the elevation angle (flight path angle) and heading angle of the relative velocity vector ($\vec{V_r}$), measured from the horizontal plane, with anti-clockwise positive angle, while α and β are the in-plane and out-of-the-plane angles, but referred to the thrust vector ($\vec{T}$), always with anti-clockwise positive angle values. The γ and ψ angles only depend on state variables, as:

$$sin\gamma = \frac{u}{V_r} \tag{5.8}$$

$$cos\gamma cos\psi = \frac{u - \omega r cos\phi}{V_r} \tag{5.9}$$

$$cos\gamma sin\psi = \frac{w}{V_r} \tag{5.10}$$

where the modulus of relative velocity (V_r) is equal to:

$$V_r = \sqrt{u^2 + (u - \omega r cos\phi)^2 + w^2} \tag{5.11}$$

The angles α and β represent the control variables that determine the direction of thrust; if we explicitly express the Hamiltonian and we nullify its partial derivatives with respect to angles α and β, we get the optimum values for these angles, which are:

$$sin\alpha = \frac{\lambda_u}{\lambda_V} \tag{5.12}$$

$$cos\alpha cos\beta = \frac{\lambda_v}{\lambda_V} \tag{5.13}$$

$$cos\alpha sin\beta = \frac{\lambda_w}{\lambda_V} \tag{5.14}$$

where:

$$\lambda_V = \sqrt{\lambda_u^2 + \lambda_v^2 + \lambda_w^2} \tag{5.15}$$

is the primer vector's modulus which is parallel to the optimal direction of thrust, as already discussed. The differential equations for the adjoint variables are obtained from the Euler-Lagrange equations, as follows:

$$\dot{\lambda}_r = \frac{1}{r^2}\left[\lambda_\vartheta \frac{v}{cos\phi} + \lambda_\phi w + \lambda_u\left(-\frac{2}{r}+v^2+w^2\right) + \lambda_v(-uv+vwtan\phi) + \lambda_w(-uw-v^2tan\phi)\right] \quad (5.16)$$

$$\dot{\lambda}_\vartheta = 0 \quad (5.17)$$

$$\dot{\lambda}_\phi = \frac{1}{rcos^2\phi}(-\lambda_\vartheta vsin\phi - \lambda_v vw + \lambda_w v^2) \quad (5.18)$$

$$\dot{\lambda}_u = \frac{1}{r}(-\lambda_r r + \lambda_v v + \lambda_w w) \quad (5.19)$$

$$\dot{\lambda}_v = \frac{1}{r}\left[-\lambda_\vartheta \frac{1}{cos\phi} - 2\lambda_u v + \lambda_v(u - wtan\phi) + 2\lambda_w vtan\phi\right] \quad (5.20)$$

$$\dot{\lambda}_w = \frac{1}{r}(-\lambda_\phi - 2\lambda_u w - \lambda_v vtan\phi + \lambda_w u) \quad (5.21)$$

$$\dot{\lambda}_v = \frac{T}{m^2}\lambda_V \quad (5.22)$$

In these equation we introduced the components of velocity with respect to the local frame of reference ZEN, that is, as already mentioned, "zenith-east-north", whose expressions are:

$$V_Z = \frac{u}{V_r} = sin\gamma \quad (5.23)$$

$$V_E = \frac{(V - \omega rcos\phi)}{V_r} = cos\gamma cos\psi \quad (5.24)$$

$$V_N = \frac{w}{V_r} = cos\gamma sin\psi \quad (5.25)$$

The switching function S_F we already mentioned earlier, determines the thruster firings, as:

$$\begin{cases} T = T_{max} & S_F > 0 \\ T = 0 & S_F < 0 \end{cases} \quad (5.26)$$

If $S_F = 0$ we will have the so-called singular arc.

In fact, if we write the Hamiltonian as:

$$H = \lambda_r{}^T V + \lambda_V{}^T g + TS_F \quad (5.27)$$

the expression of the switching function will be:

$$S_F = \frac{\lambda_V}{m} - \frac{\lambda_m}{c} \quad (5.28)$$

Chapter 6

Method of resolution

The indirect method on which the procedure of optimization of interplanetary trajectories is based starts from the theory of optimal control, which will be applied to the equations' system reported above, whose boundary conditions depend on the type of initial and final orbit, between which the transfer orbit is performed. [2]

The theory of optimal control formulates a new system of boundary value problem (BVP), in which some of the initial variables' values are unknown. The solution to this problem consists in finding a set of initial values which allows, after numerically integrating the differential system, to satisfy all the boundary conditions, either imposed or optimum conditions.

As exposed in the previous chapter, the theory of optimal control formulates the optimum problem as a mathematical problem, subject to differential and algebraic constraints. Given that some of the initial values of the state and adjoint variables are unknown, the optimum problem becomes a boundary values problem (BVP).

It is important to notice that the problem we are solving has some peculiarities, such as:

- the integration interval is divided into sub-intervals in which the differential equation can have different expressions;

- the duration of each interval is unknown;

- the boundary conditions can be non-linear and they can involve the variable values both in the internal or external boundaries;

- the variable can be discontinuous at the internal boundaries and their values right after the discontinuity can be unknown.

In order to solve the boundary values problem yet discussed, it is reformulated as a series of initial values problems, whose convergence is reached by the Newton method. As already mentioned, the duration of each interval is unknown, therefore, in order to solve this indetermination, we can replace the independent variable t with a new variable, ε, defined at the j-th interval as:

$$\varepsilon = j - 1 + \frac{t - t_{j-1}}{t_j - t_{j-1}} = j - 1 + \frac{t - t_{j-1}}{\tau_j} \tag{6.1}$$

with τ_j defined as the duration of j-th interval, generally unknown. It is possible to notice that, after this substitution, the internal and external intervals are fixed in terms of time, thanks to

the introduction of the unknown variables τ_j. At the beginning or at the end of each interval, the new variable ε assumes integer values, as it is easily verifiable.

We can therefore rewrite the system yet introduced in the previous chapter, also including the adjoint variables λ, thus defining the vector $y = (x, \lambda)$, as follows:

$$\frac{dy}{dt} = \boldsymbol{f}^*(y, t) \tag{6.2}$$

but this last formalism does not take into account the constant values we encountered so far, such as the interval durations τ_j, or the variables values after a discontinuity, so we can introduce a new vector, called z, which include the variables y and the constants c:

$$\frac{dz}{d\varepsilon} = \boldsymbol{f}(z, \varepsilon) \tag{6.3}$$

If we refer to the vector containing the state variables and the adjoint variables, we can rewrite the first member of the last equation in function of ε. In the case of variables, we have:

$$\frac{dy}{d\varepsilon} = \tau_j \frac{dy}{dt} \tag{6.4}$$

while, for the constants vector:

$$\frac{dc}{d\varepsilon} = 0 \tag{6.5}$$

The boundary conditions, both imposed and optimum conditions, are formalized as:

$$\Psi(s) = 0 \tag{6.6}$$

with s representing a vector that includes the variables (state and adjoint variables) and the constants c, such that we can mathematically express it as:

$$s = (y_0, y_1, ..., y_n, c) \tag{6.7}$$

The initial values of some variables are unknown, thus the research of the solution is meant to be an iterative process of determination of these values, in order to satisfy the boundary condition expressed by the formalism above. If we assume that none of the values is known, we can say that the r-th iteration starts with the integration of the equation from the values found in the previous iteration p^r; we can express this last step as follows:

$$z(0) = p^r \tag{6.8}$$

The integration of the equations is performed for all the intervals at the same time, taking into account possible discontinuities within the subintervals and, in order to start the iterative process, a set of tentative values has to be chosen (p^1). For each boundary, the value of the variables is calculated, and after integrating, the errors on the boundary conditions (Ψ^r) at the r-th iteration are evaluated.

A Δp variation on the boundary conditions leads to a variation of the errors that is, taking into account only the first order terms, equal to:

$$\Delta \Psi = \left[\frac{\partial \Psi}{\partial p} \right] \Delta p \tag{6.9}$$

so, in order to nullify the errors of the boundary conditions, which mathematically means that $\Delta \Psi = -\Psi^r$, at each step of the iteration the initial values are corrected by a quantity Δp such that:

$$\Delta p = p^{r+1} - p^r = \left[\frac{\partial \Psi}{\partial p} \right]^{-1} \Psi^r \tag{6.10}$$

until the boundary condition are satisfied with the desired tolerance. The matrix appearing in the last equation is evaluated as follows:

$$\left[\frac{\partial \Psi}{\partial p} \right] = \left[\frac{\partial \Psi}{\partial s} \right] \left[\frac{\partial s}{\partial p} \right] \tag{6.11}$$

The first of the two matrices appearing at the second member of the last equation can be obtained by deriving the boundary conditions with respect to the variables, while the second matrix, which contains the derivatives of the values of the boundary conditions with respect to the initial conditions, contains the values of the variables at the boundaries assumed by the matrix:

$$\left[\frac{\partial z}{\partial p} \right] = [g(\varepsilon)] \tag{6.12}$$

is obtained by integrating the differential equations system 6.3 which, on its hand, is computed by deriving the main system with respect to each of the initial values:

$$[\dot{g}] = \frac{d}{d\varepsilon} \left[\frac{\partial z}{\partial p} \right] = \left[\frac{\partial}{\partial p} \left(\frac{dz}{d\varepsilon} \right) \right] = \left[\frac{\partial f}{\partial p} \right] \tag{6.13}$$

where the dot above the function g indicates the derivative with respect to the new independent variable ε. If we explicitly express the Jacobian of the main system (equation 6.3), the last equation can be written as:

$$[\dot{g}] = \left[\frac{\partial f}{\partial z} \right] \left[\frac{\partial z}{\partial p} \right] = \left[\frac{\partial f}{\partial z} \right] [g] \tag{6.14}$$

The initial values of the homogeneous system right above are evaluated by deriving the former relation 6.8, thus obtaining the identity matrix:

$$[g(0)] = \left[\frac{\partial z(0)}{\partial p} \right] = [\mathbf{I}] \tag{6.15}$$

Moreover, it is possible to handle the discontinuities of the variables on the generic i point, just by updating the variables vector z and the matrix g through the relation h, which relates the values of the variables before and after the discontinuities:

$$z_{i+} = h(z_{i-}) \tag{6.16}$$

$$[g_{i+}] = \left[\frac{\partial h}{\partial z}\right][g_{i-}] \tag{6.17}$$

It is important to specify that, if some of the variables defining the system are already known, the problem is limited to the unknown variables, thus simplifying the calculations.

The matrix $\left[\frac{\partial \Psi}{\partial p}\right]^{-1}$ can be evaluated also numerically: in fact the i-th row can be calculated by varying the i-th component of p of a small quantity Δp, with all the other variables fixed, then integrating the equations. It is thus possible to determine the boundary conditions corrections $\Delta\Psi(\Delta p)$ and, after linearizing, get the corresponding row as $\Delta\Psi^T/\Delta p$. The same procedure can be exploited to calculate the Jacobian and the matrix $[\partial\Psi/\partial s]$. Nevertheless, in both cases, this evaluation can be imprecise and the convergence is not guaranteed, as the introduced approximations may compromise the convergence itself.

Analogously, the linearization that has been introduced to evaluate the corrections Δp to be applied to the tentative solutions, given by the former equation, introduces errors that can compromise the convergence of the iterations, in the same way. Therefore, the procedure of tentative solution's correction has here received some corrections. We can summarize them with the following points:

- in order not to move away from the solution, the actual correction is a fraction of the calculated one, so:

$$p^{r+1} = p^r + K_1\Delta p$$

  with $K_1 = 0.1 \div 1$ that is empirically determined in the first trials of the codes, depending on the goodness of the first solution;

- at each iteration, after determining the initial values vector and integrating the equations of motion, the maximum error on the boundary conditions E_{max}^{r+1} is compared with the maximum error at the previous iteration E_{max}^r. If the error is lower than a multiple of the previous error, $E_{max}^{r+1} < K_2 E_{max}^r$, then the iteration process goes on. As the error can increase in the first steps, the proper value of K_2 is greater than the unity; normally values of K_2 range between 2 and 3;

- if, conversely, the error on the r-th iteration is too much greater than the previous one's, a bisection will be applied on the correction itself, thus resulting a correction whose values are half of the original one's. Thus, the new tentative solution will be equal to:

$$p^{r+1} = p^r + K_1\Delta p/2$$

The corrections' comparison process goes on until the maximum number of iterations on one tentative solution is reached; after that, the iterations stop and a new first tentative solution is introduced.

In order to make the results readable, it is necessary to specify the value of two adimensional quantities to which we will refer. In fact:

- the times of the mission will be measured by an angular quantity, which relation with time measured in years is:
$$2\pi = 1 year$$

- the distances of the mission will be measured by an adimensional quantity, the *astronomical unit*, whose unit value is:

$$1 AU = 149\,597\,870.691\,\text{km}$$

which is the mean distance between Earth and Sun;

- the times of the mission are measured starting from the $t_0 = 0$, which corresponds to the date of 1st January 2000.

Chapter 7

Results

The results of the simulations carried out using the methods discussed in the previous chapters are presented in the following sections. The characteristic parameter of the spacecraft we are considering (initial mass, power, thrust, exhaust velocity, specific impulse) are reported in the table down below:

Table 7.1: Values of initial mass, power, thrust, exhaust velocity and specific impulse for the selected engine.

Parameter	m_0	P	T	c	I_{sp}
Value	20 kg	26.4485 W	0.001 74 N	30.401 km/s	3100 s

7.1   Missions to real asteroids

The simulations, whose results are given and commented on in this section, were conducted using ten asteroids selected among the NEAs described in Chapter 2 without changing the orbital parameters and thus utilizing the original values in the code database. For all the simulated missions, a fixed duration of 2 years has been imposed. The trend of the angles alpha and beta, already defined in Chapter 5 as the in-plane and out-of-the-plane angles, referred to the thrust vector, as well as the final masses of the spacecraft, from which all of the observations and hypotheses object of this thesis were obtained, appear to be particularly significant. Before moving to the results, it is meaningful to have a look at the asteroids' orbital parameters collected in the table below, in order to better understand the different results according to the considered asteroid.

Table 7.2: Orbital parameters of the Earth and the ten selected asteroids.

Asteroid	a [UA]	e	ι [deg]	Ω [deg]	ω [deg]	r_p [UA]	r_a [UA]
Earth	0.9999	0.0167	0.00099	175.406	287.616	0.9832	1.0164
2016 TB57	1.1022	0.1232	0.2983	147.798	294.83	0.9665	1.2380
2013 WA44	1.10046	0.0605	2.302	176.731	56.513	1.0339	1.1670
2013 BS45	0.9917	0.08375	0.77255	150.694	83.365	0.9087	1.0748
2015 BM510	0.9468	0.1215	1.58896	357.341	267.875	0.8317	1.0619
2014 SD304	1.1678	0.10838	2.29384	19.2989	7.6281	1.0413	1.2945
2012 EC	1.1516	0.13742	0.9135	333.906	306.079	0.9934	1.3099
2009 CV	1.1158	0.1507	0.9427	181.3579	22.401	0.9476	1.2839
2016 CF137	1.0904	0.1001	2.4447	301.495	132.547	0.9813	1.1996
2014 YD	1.0721	0.08662	1.73574	34.116	117.64	0.9793	1.1650
2009 OS5	1.1443	0.09678	1.6952	120.852	145.3602	1.0335	1.2550

7.1.1 Final mass values and trends of α and β

In the table below, the values of initial and final times, together in the values of final masses are reported, followed by graphs showing the trends of angles alpha and beta for each asteroid, as already discussed.

Table 7.3: Values of initial times, final times and final masses of mission toward the ten selected asteroids.

| Asteroid	t_0	t_f	m_f/m_0
2016 TB57	175.7949	188.3613	0.94086
2013 WA44	162.78713	175.3535	0.93761
2013 BS45	164.44635	177.0127	0.94957
2015 BM510	167.24377	179.81014	0.92181
2014 SD304	171.54092	184.10729	0.91508
2012 EC	173.02293	185.5893	0.89472
2009 CV	176.63615	189.20252	0.91818
2016 CF137	178.94067	191.50704	0.92772
2014 YD	181.48851	194.05488	0.94444
2009 OS5	181.99586	194.56223	0.92521
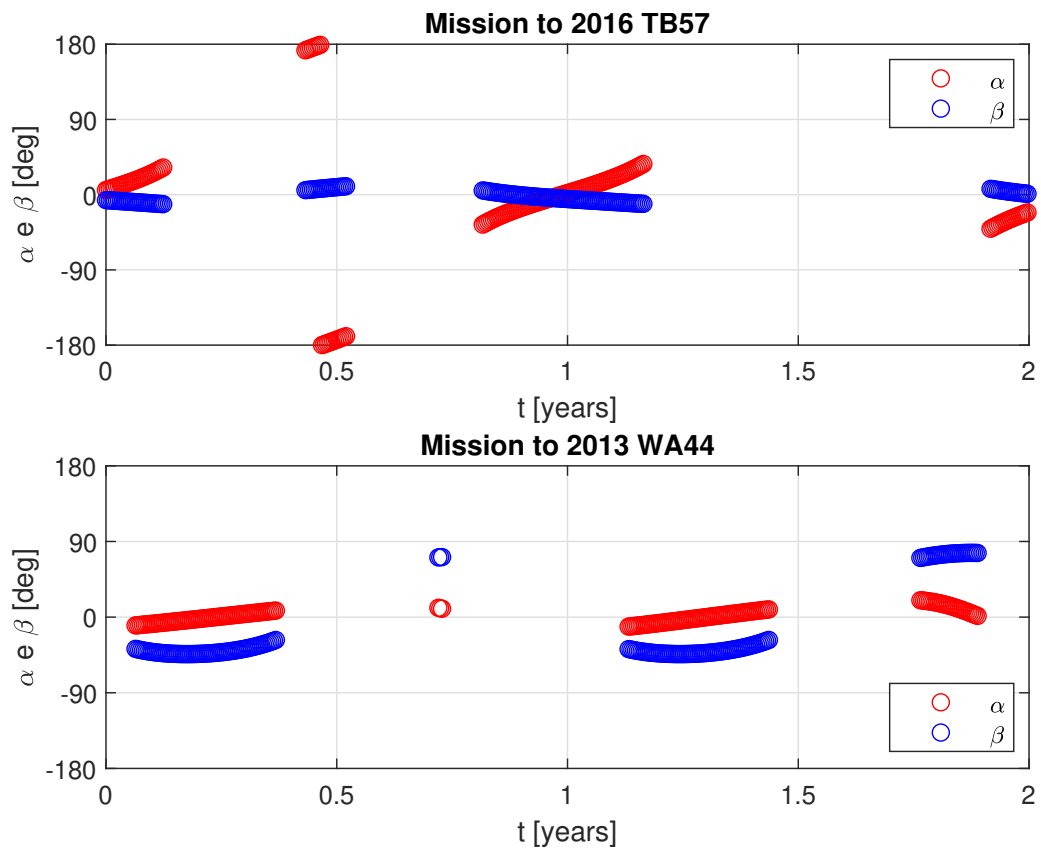
Figure 7.1: Trends of alpha and beta for asteroids 2016 TB57 and 2013 WA44.
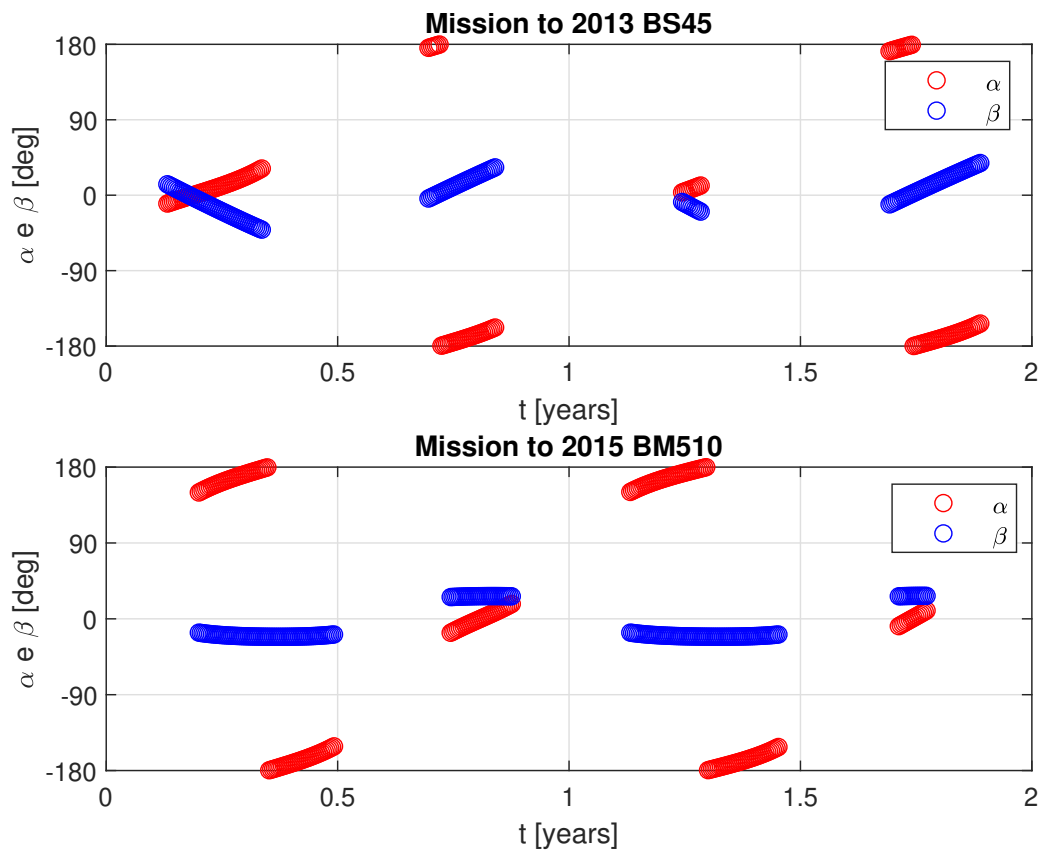
Figure 7.2: Trends of alpha and beta for asteroids 2013 BS45 and 2015 BM510.
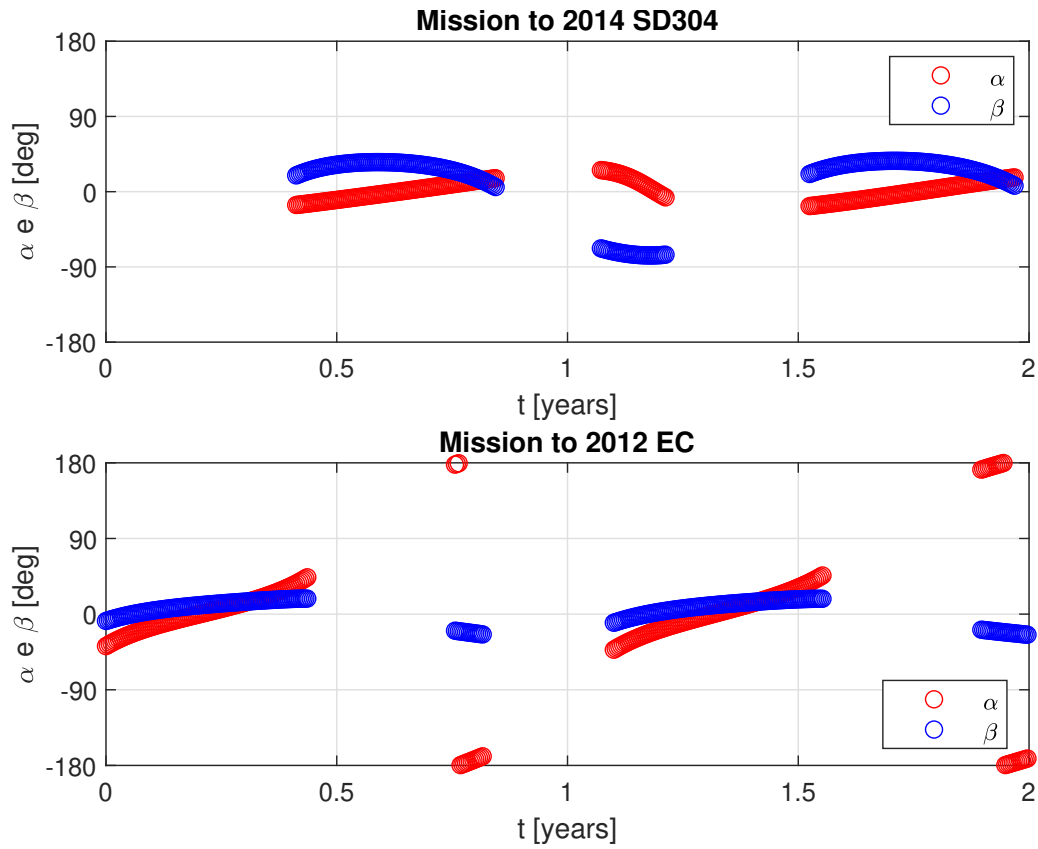
Figure 7.3: Trends of alpha and beta for asteroids 2014 SD304 and 2012 EC.
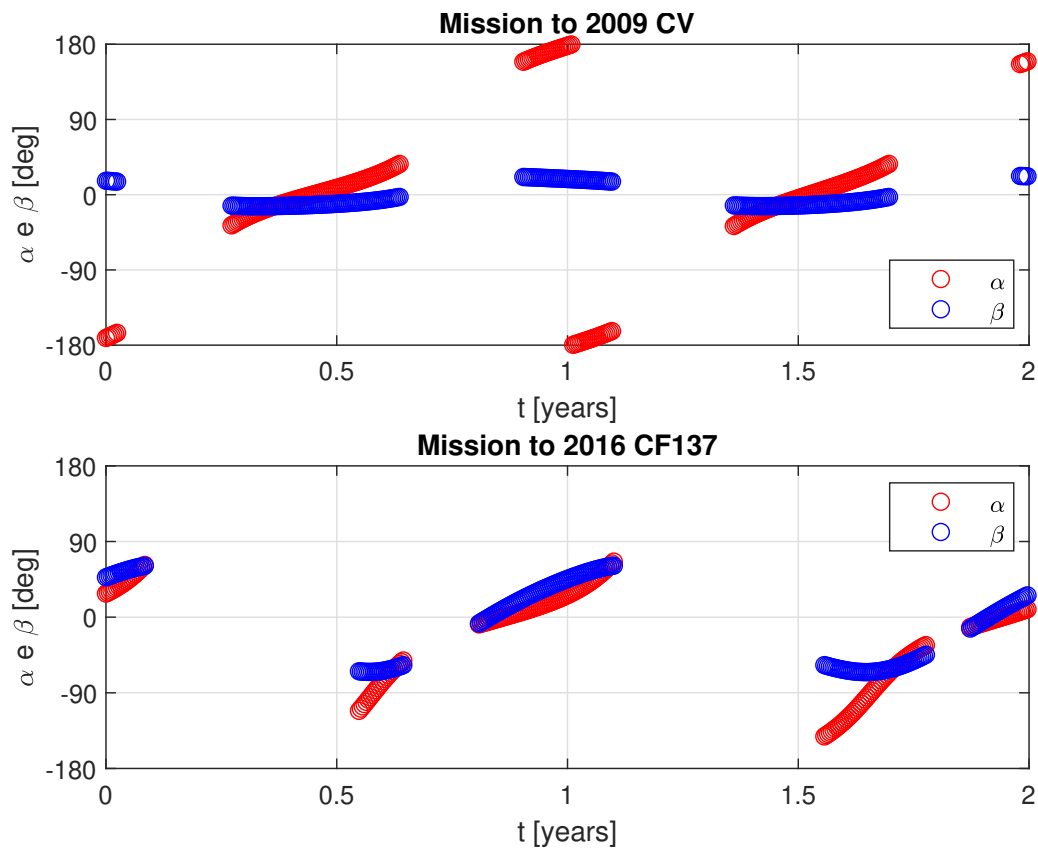
Figure 7.4: Trends of alpha and beta for asteroids 2009 CV and 2016 CF137.
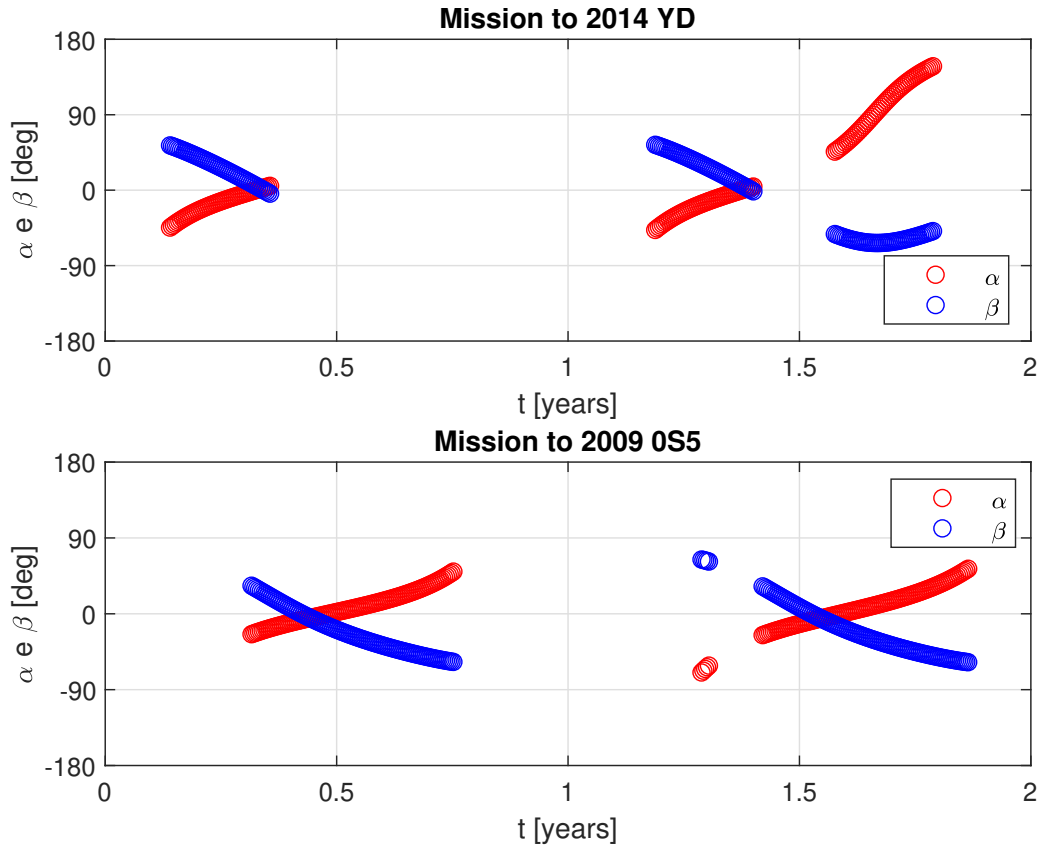
Figure 7.5: Trends of alpha and beta for asteroids 2014 YD and 2009 OS5.

7.1.2 Comments and observations

From the graphs shown above, it appears evident that two distinct types of missions can be distinguished, each of which differs and is defined by the following factors:

- **Type A**: including asteroids 2016 TB57, 2013 WA44, 2013 BS45, 2015 BM510, 2014 SD304, 2012 EC and 2009 CV that are characterized by the application of thrust occurring at regular intervals of time, with the mean value of the angle alpha for each interval being close to zero;

- **Type B**: including asteroids 2016 CF137, 2014 YD and 2009 OS5, in which it is clear that the engine's firing intervals are irregular and unequal, and that the mean values of the angle alpha depart from the null value in a meaningful way.

Moreover, we can observe that the greater the Δa's, Δe's and/or $\Delta \iota$'s are, the least the final masses are. This was expected to occur, as it is known from astrodynamics that, in a one-impulse maneuver, the ΔV's are directly proportional to these three quantities.

7.2 Possible explanations to type B asteroids' behavior

In order to give an explanation of the behavior of asteroids of type B, it is useful to look up three important quantities Δa, Δe, Δi, Δr_p and Δr_p, which are the differences between asteroids' semi-major axes, eccentricities, inclinations and absides' radii and the Earth's values, which are reported in the following table, together with the ones of type A. The asteroids of type B are highlighted in red.

Table 7.4: Differences between asteroids' and Earth's orbital parameters.

Asteroid	$|\Delta a|$ [UA]	$|\Delta e|$	$|\Delta\iota|$ [deg]	$|\Delta r_p|$ [UA]	$|\Delta r_a|$ [UA]
2016 TB57	0.1022528	0.106455	0.29734	0.0167	0.2216
2013 WA44	0.1004717	0.0437583	2.30121	0.0507	0.1506
2013 BS45	0.0082544	0.0670329	0.77156	0.0745	0.0584
2015 BM510	0.0531796	0.10481662	1.58797	0.1515	0.0455
2014 SD304	0.1678941	0.09166632	2.29285	0.0581	0.2781
2012 EC	0.1516615	0.12070851	0.91247	0.0102	0.2935
2009 CV	0.1157751	0.13401057	0.94171	0.0356	0.2675
2016 CF137	0.09045929	0.0834084	2.44375	0.0019	0.1832
2014 YD	0.072156	0.0699032	1.73475	0.0039	0.1486
2009 OS5	0.144276	0.0800615	1.69425	0.0503	0.2386

It is possible to notice that the differences of semi-major axes of two asteroids from type B, 2016 CF137 and 2014 YD, are very limited, as they are lower than a percentage of 10 %, while the third asteroid, 2009 0S5, reaches a Δa value of 0.144. The differences in the eccentricities of the aforementioned asteroids are quite high, therefore these two properties affect the perihelia and aphelia radii. In fact, it is clear that differences of the perihelion radii of asteroids 2016 CF137 and 2014 YD with respect to the Earth's one, are very low, even lower than a percentage of 1 %, while the third type B asteroid, 2009 OS5, reaches a difference of perihelion radius slightly greater than a 5 %. Additionally, all three of the aforementioned asteroids have inclinations that are significantly higher than zero and, as a consequence, their inclinations' differences will be quite high.

Table 7.5: Longitudes of ascending nodes and perihelion of Earth and asteroids.

Asteroid	Longitude of ascending node	Longitude of perihelion
Earth	175.40 deg	103.02 deg
2016 TB57	147.79 deg	82.62 deg
2013 WA44	176.73 deg	233.24 deg
2013 BS45	150.69 deg	234.05 deg
2015 BM510	357.34 deg	265.21 deg
2014 SD304	19.29 deg	26.92 deg
2012 EC	333.90 deg	279.98 deg
2009 CV	181.35 deg	203.75 deg
2016 CF137	301.49 deg	74.042 deg
2014 YD	34.11 deg	151.75 deg
2009 OS5	120.85 deg	266.21 deg

In addition, if we take a look at the table above, we can take into consideration one asteroid from type B, for example 2016 CF137, and one from type A, for example 2012 EC, in order to make a comparison between these two and find out more information to get to the main cause of these differences. The most interesting parameter appears to be the longitude of perihelion:

in fact, starting from a value of longitude Earth's perihelion approximately close to 90 degrees, asteroid 2016 CF137 from type B has a similar value of the aforementioned parameter, while asteroid 2012 EC from type A has a perihelion whose longitude is close to 270 degrees. This means that the 2012 EC's perihelion is 180 degrees far from the Earth's one.

Furthermore, it is significant to investigate where the engine firings occur in terms of the longitude of the spacecraft on its orbit, that is to better understand whether they take place near the line of nodes or near the absides line. In fact, it is known from orbital mechanics that it is convenient to make a plane change maneuver on the line of nodes, while it is better to make an abside adjustment maneuver on the line of abside. Therefore, the greater the inclination of the target is, the more engine firings will occur near the line of nodes; conversely, if most of the firings result near the line of absides, then the importance of the semi-major axis in the optimization of mass will be higher.

From the graphs reported below, it is possible to observe that:

- the firing arches are centered on the absides (aphelion or perihelion) and the angle α centered on 0 or 180 degrees for a small asteroid's orbit inclination or, alternatively, if the inclination is quite great but the argument of periapsis is close to 0 or 180 degrees;

- the firing arches are centered on the line of nodes (with a consequent lower final mass) if the argument of periapsis is close to 90 or 270 degrees.
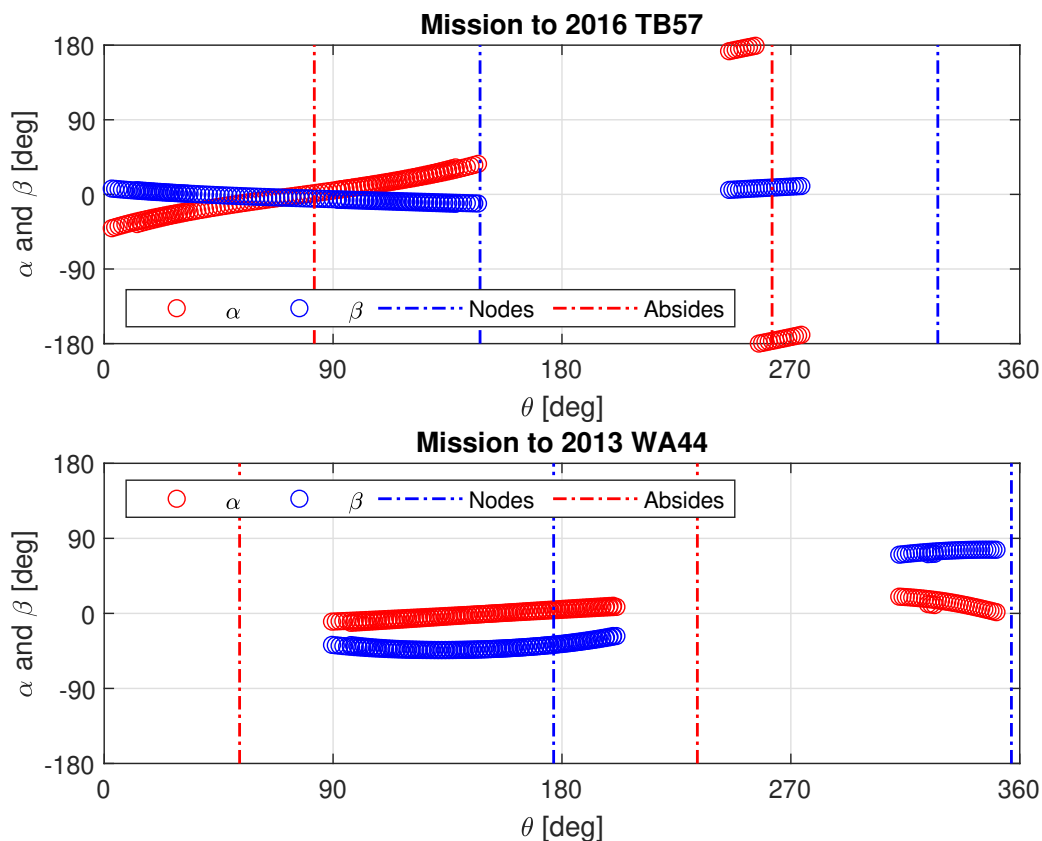
Figure 7.6: Trends of alpha and beta in function of theta for 2016 TB57 and 2013 WA44.
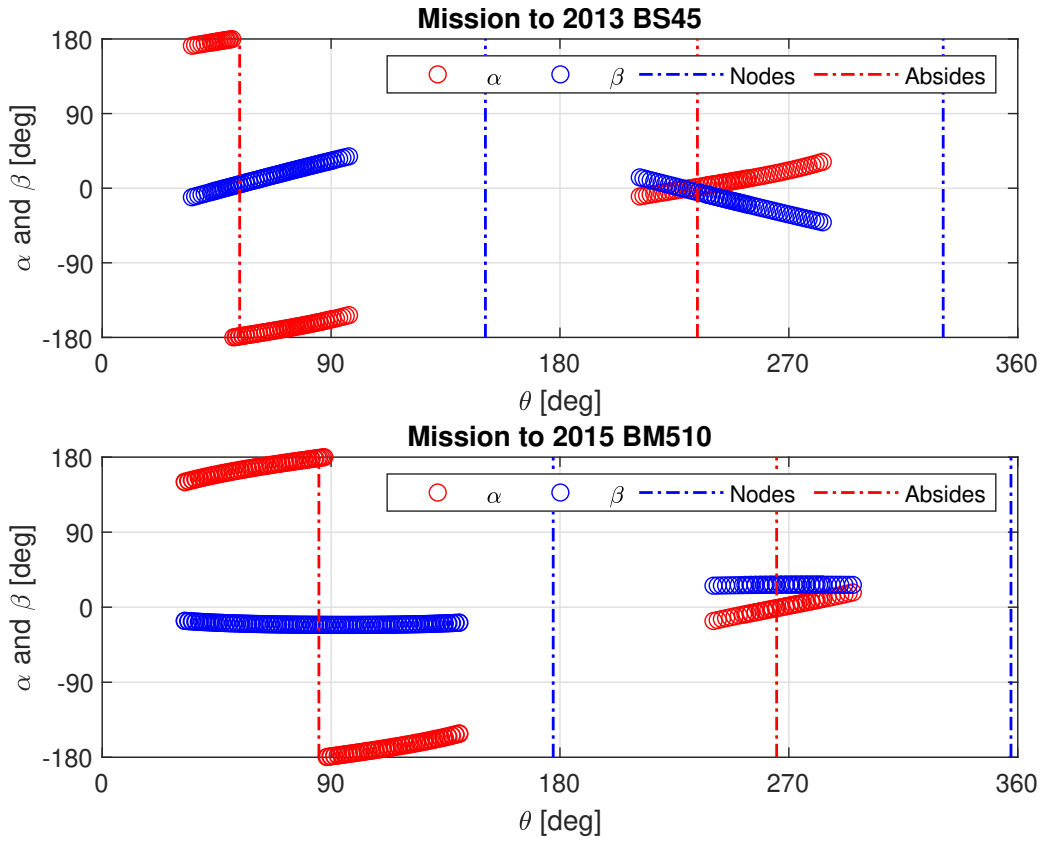
Figure 7.7: Trends of alpha and beta in function of theta for 2013 BS45 and 2015 BM510.
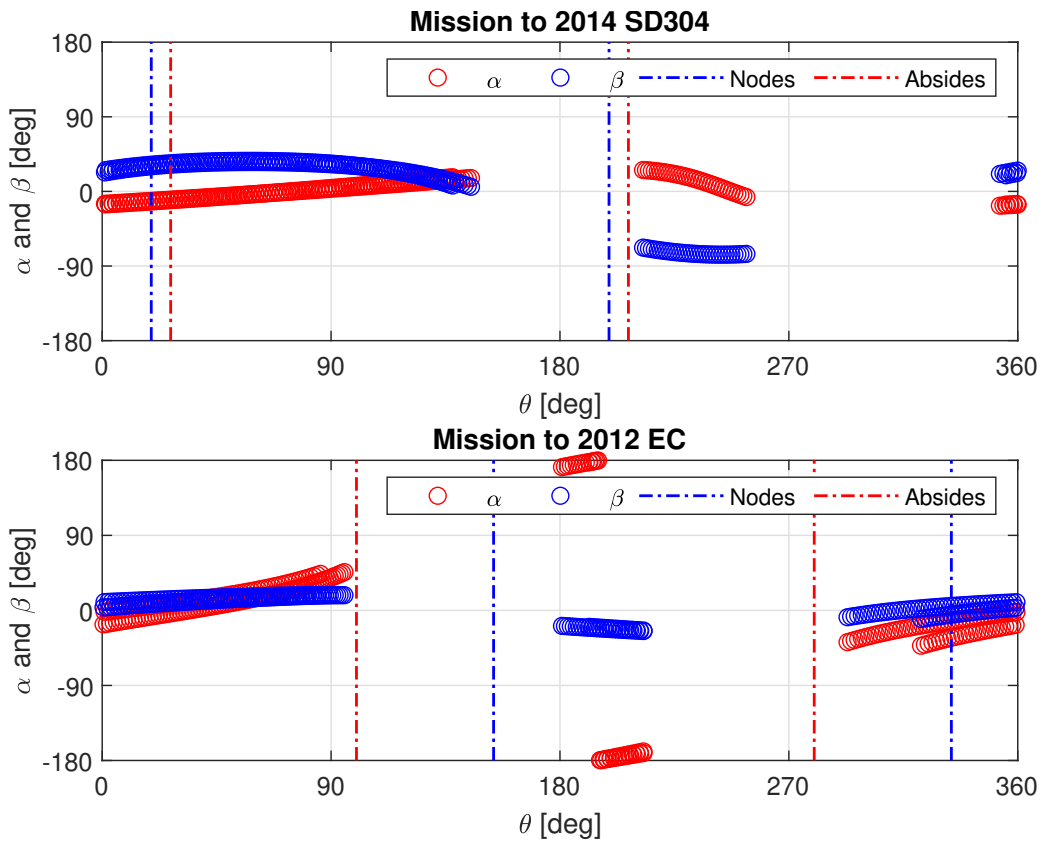

Figure 7.8: Trends of alpha and beta in function of theta for 2014 SD304 and 2012 EC.
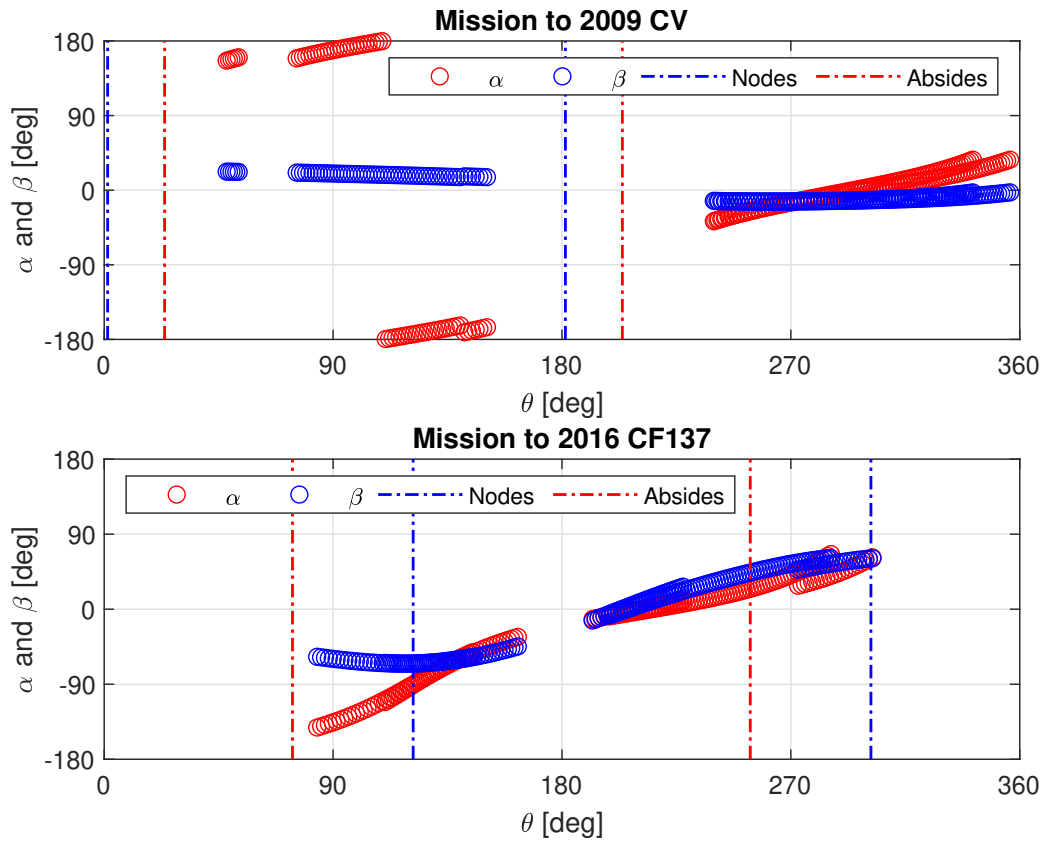
Figure 7.9: Trends of alpha and beta in function of theta for 2009 CV and 2016 CF137.
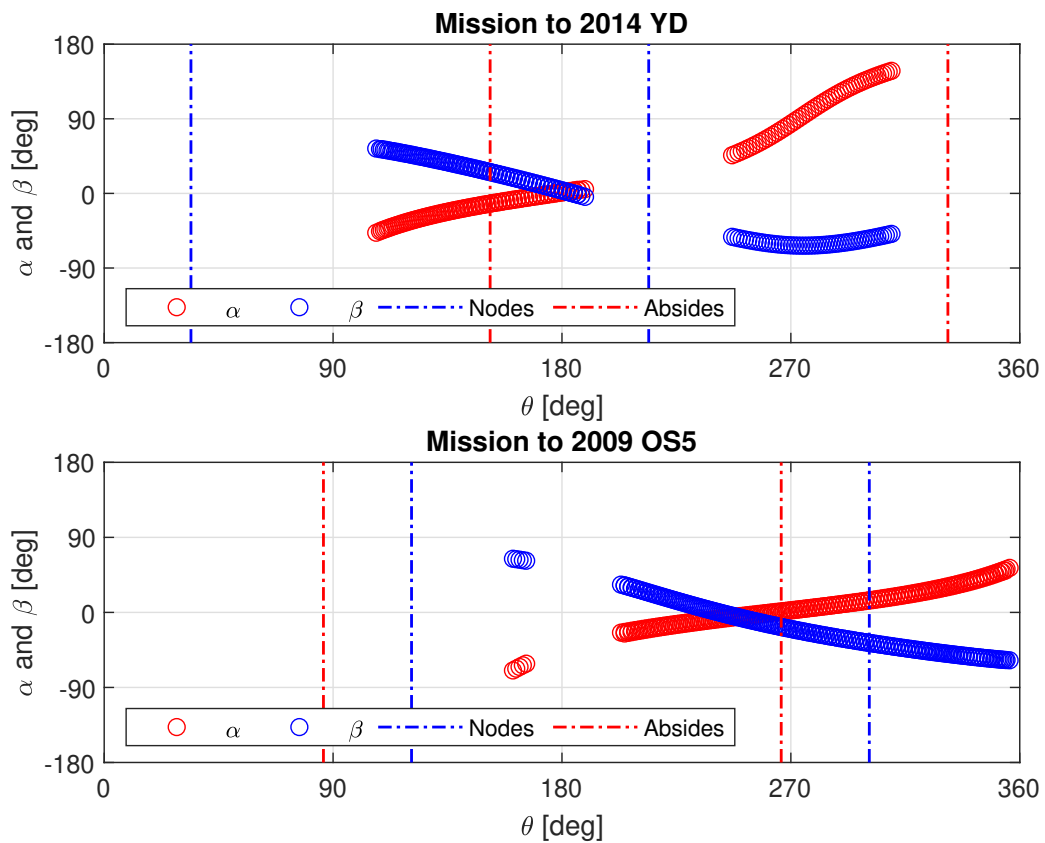

Figure 7.10: Trends of alpha and beta in function of theta for 2014 YD and 2009 0S5.

Two last parameters whose trends are interesting to investigate are the perihelion and the aphelion radii in function of time. In fact, from the graphs it is possible to notice that, during a mission toward asteroids from type A, the spacecraft varies its perihelia and aphelia radii separately, therefore maneuvers aiming to adjust one or the other abside occur at different times. On the contrary, asteroids from type B show a series of variations of the absides in the same instants of time. These last observations are true only if we neglect some initial instants, when asteroids from type A show coupled variation of r_p and r_a. This last phenomenon is likely due to the Earth's eccentricity.
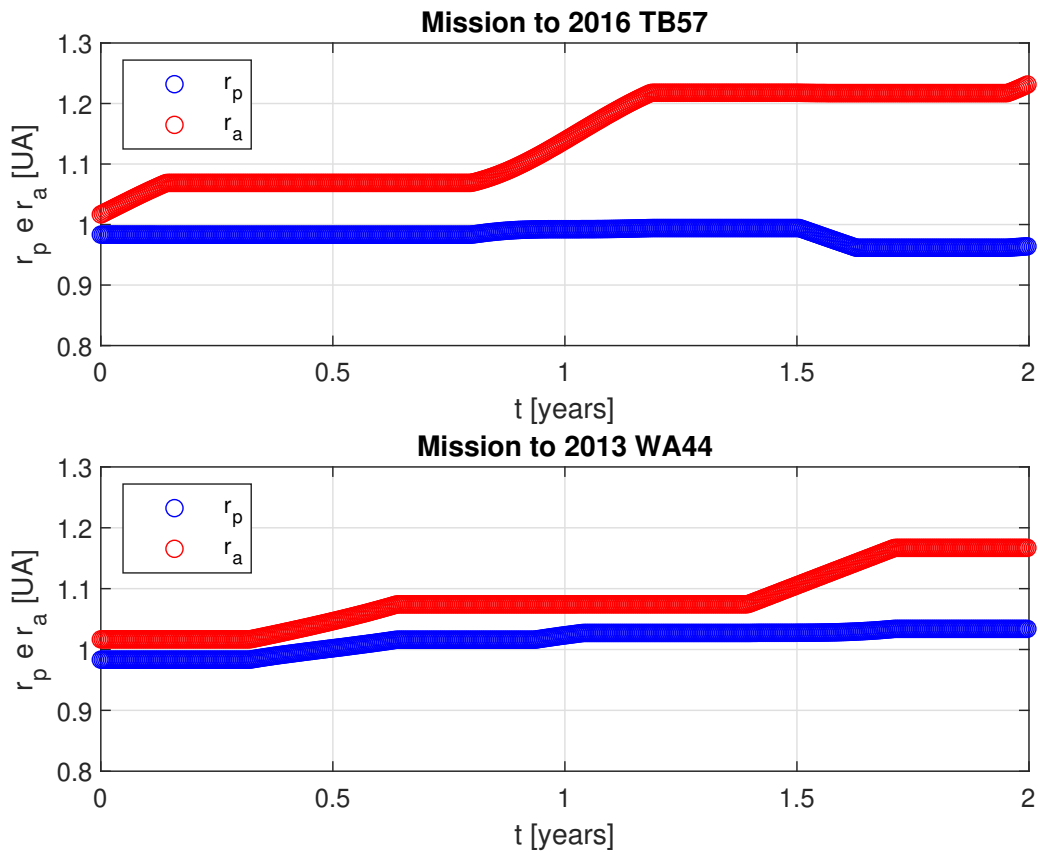
Figure 7.11: Trends of aphelion and perihelion radius for 2016 TB57 and 2013 WA44.
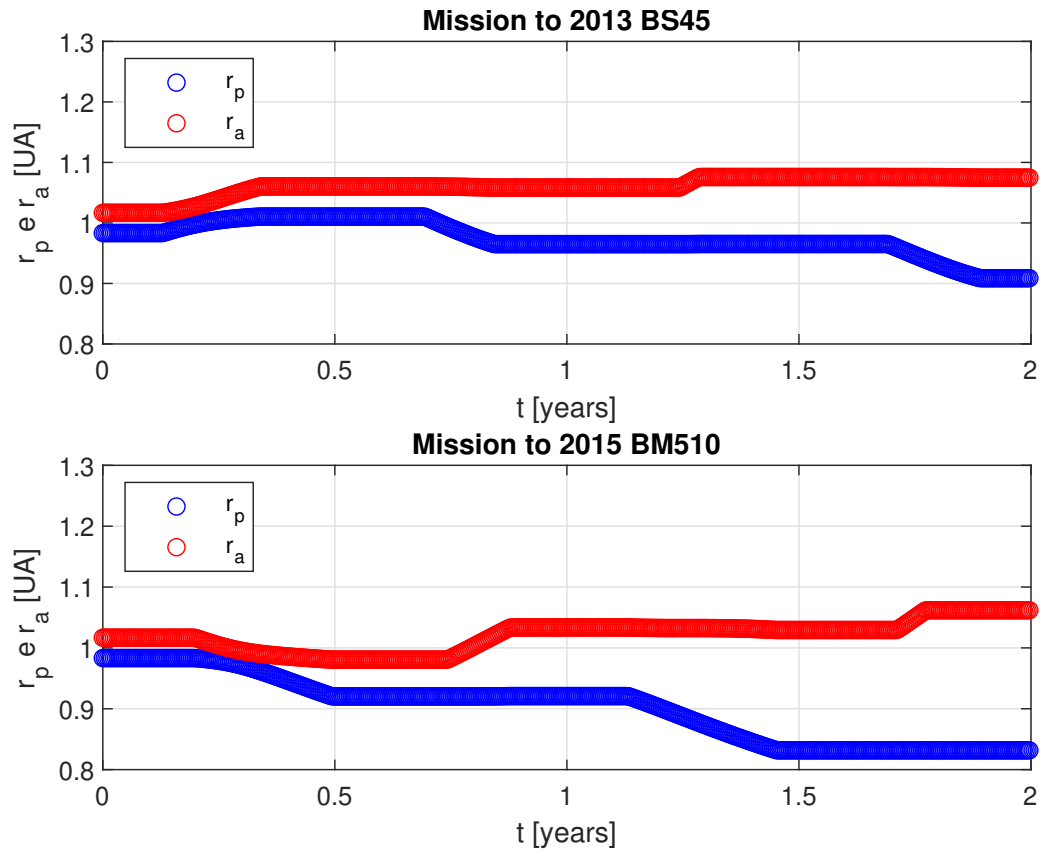
Figure 7.12: Trends of aphelion and perihelion radius for 2013 BS45 and 2015 BM510.
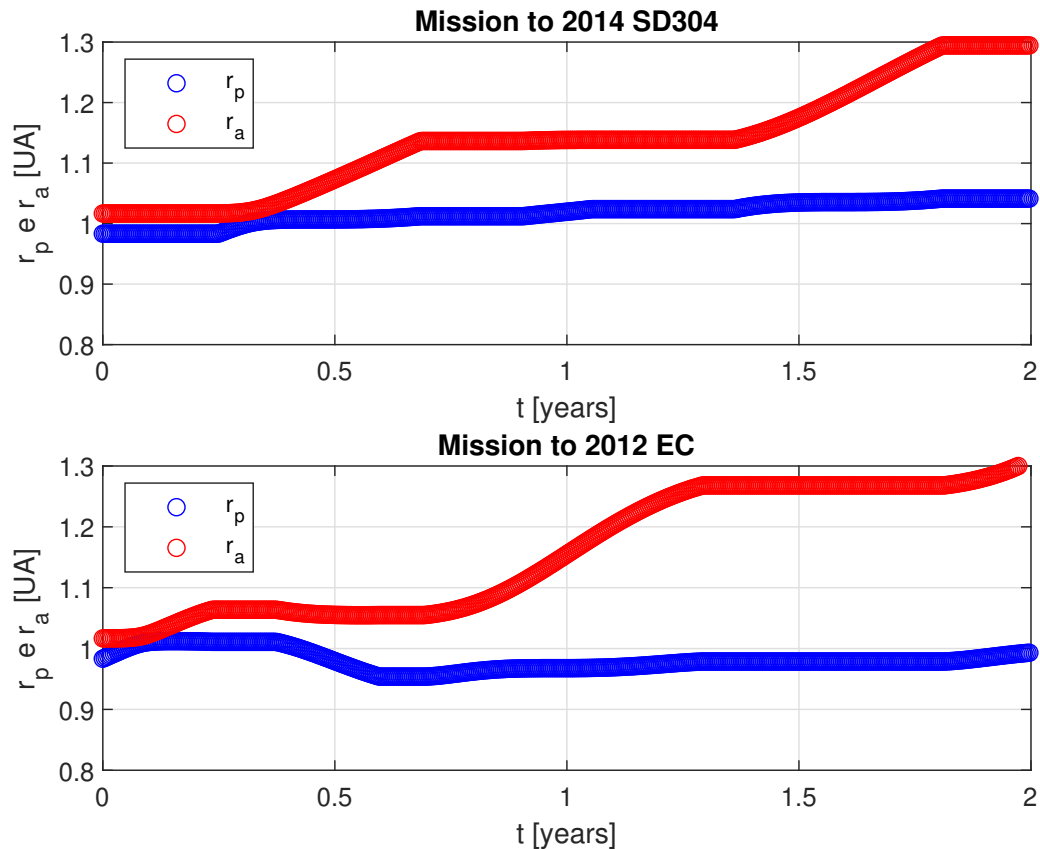
Figure 7.13: Trends of aphelion and perihelion radius for 2014 SD304 and 2012 EC.
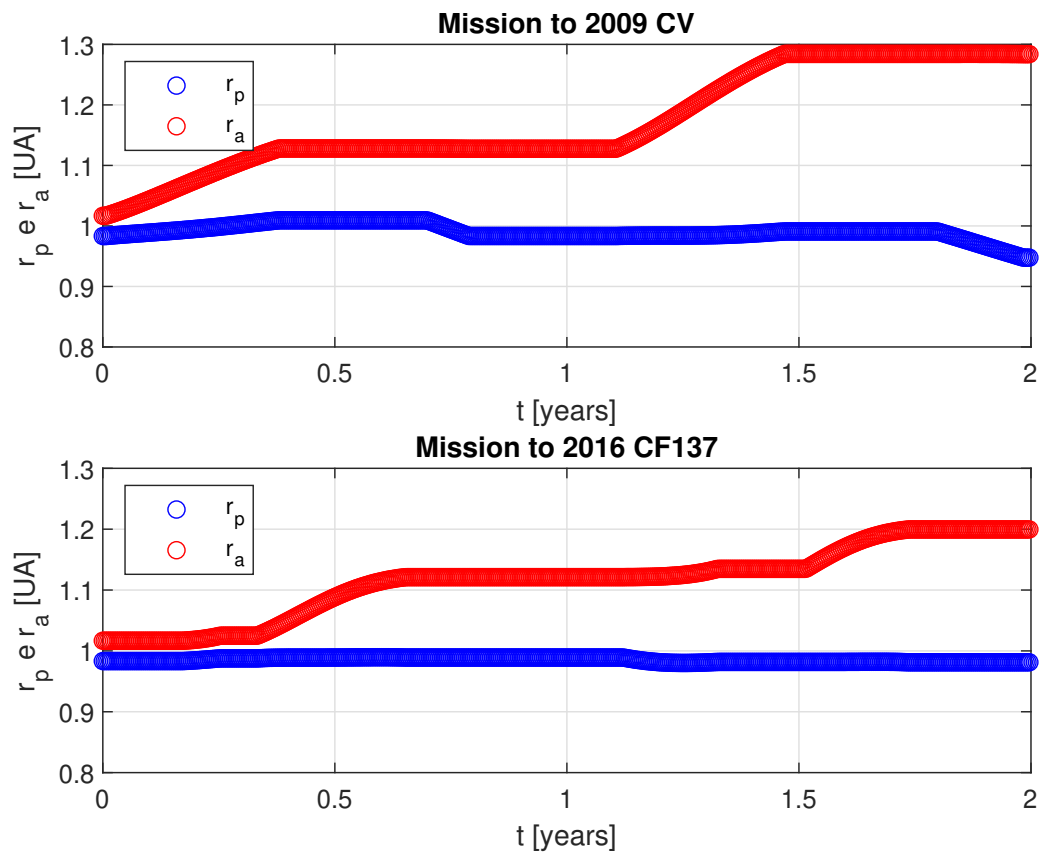
Figure 7.14: Trends of aphelion and perihelion radius for 2009 CV and 2016 CF137.
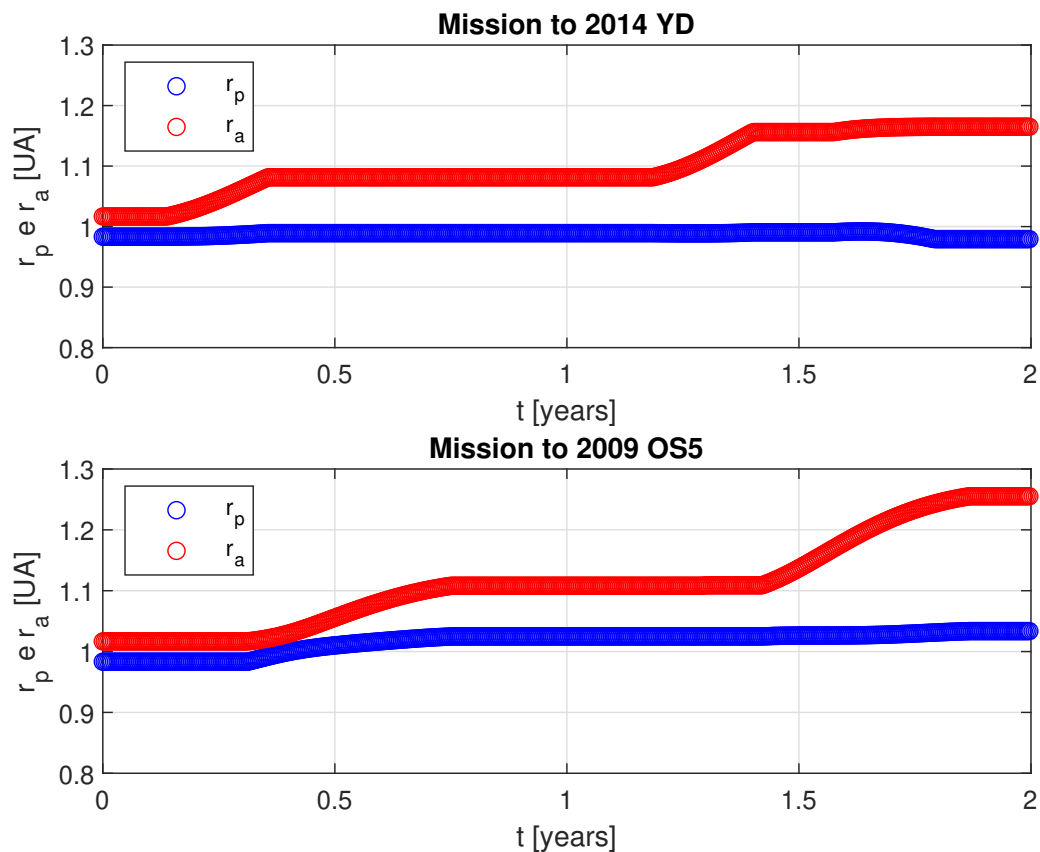

Figure 7.15: Trends of aphelion and perihelion radius for 2014 YD and 2009 OS5.

Summarizing the previous results, we can formulate some hypotheses to explain the different behaviors of asteroids from the two types:

- type B behavior is given by high values of either Δe and Δi, while Δa differences are limited. This results in perhelion radii values that are very close to the Earth's one;

- values of perihelion longitudes clearly affect trends of alpha and beta angles, as asteroids' perihelion values close to the Earth one determine a behavior similar to type B asteroids, while values which are 180 degrees far from the Earth one lead to a type A behavior;

- perihelion radii close to the Earth's one leads to a type B behavior.

7.3 Missions to modified asteroids and hypotheses testing

In this section, the hypotheses exposed right above will be tested, in order to confirm or invalidate them. For this purpose, one asteroid from type A (2012 EC) and one from type B (2016 CF137) will be considered and some of their and Earth's orbital parameters will be varied in order to evaluate the effect that each one has on mission performances. The first parameter to be tested is the Earth's eccentricity, then to demonstrate that a high eccentricity affects aphelion and perihelion radii thus determining a type B behavior, the Earth's eccentricity is imposed equal to zero.
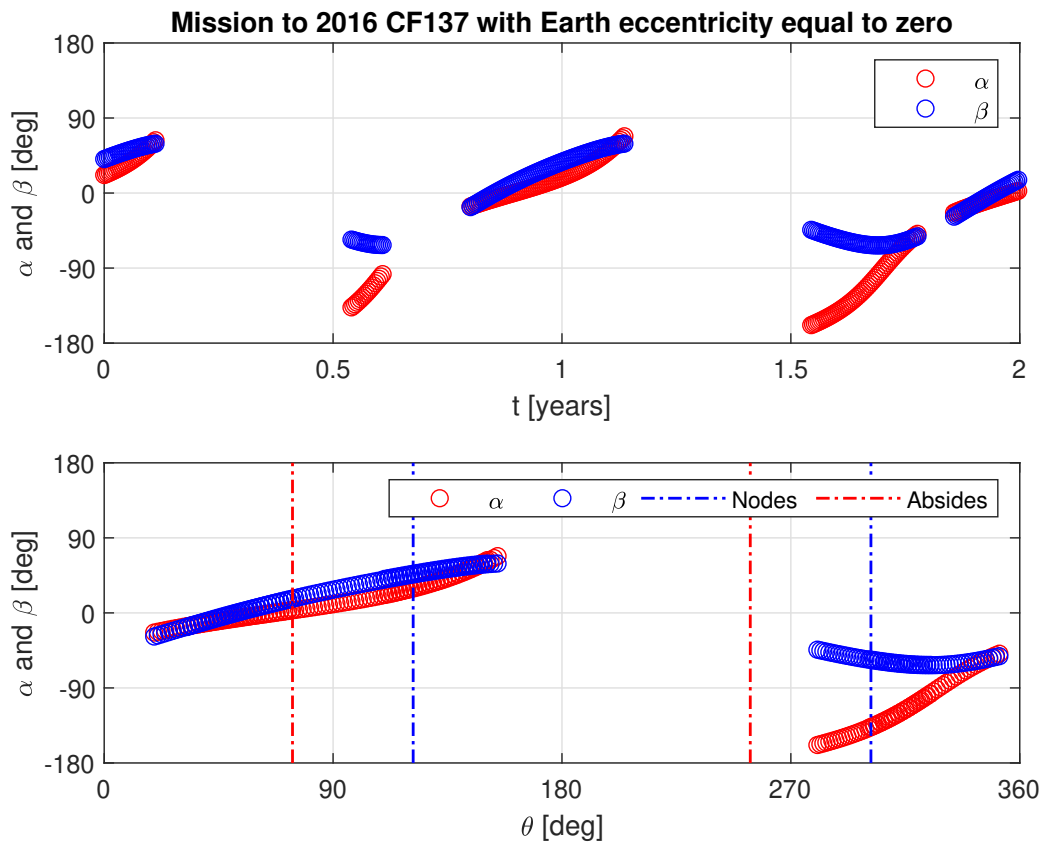

Figure 7.16: Trends of alpha, beta and theta for 2016 CF137 with $e_{Earth} = 0$.
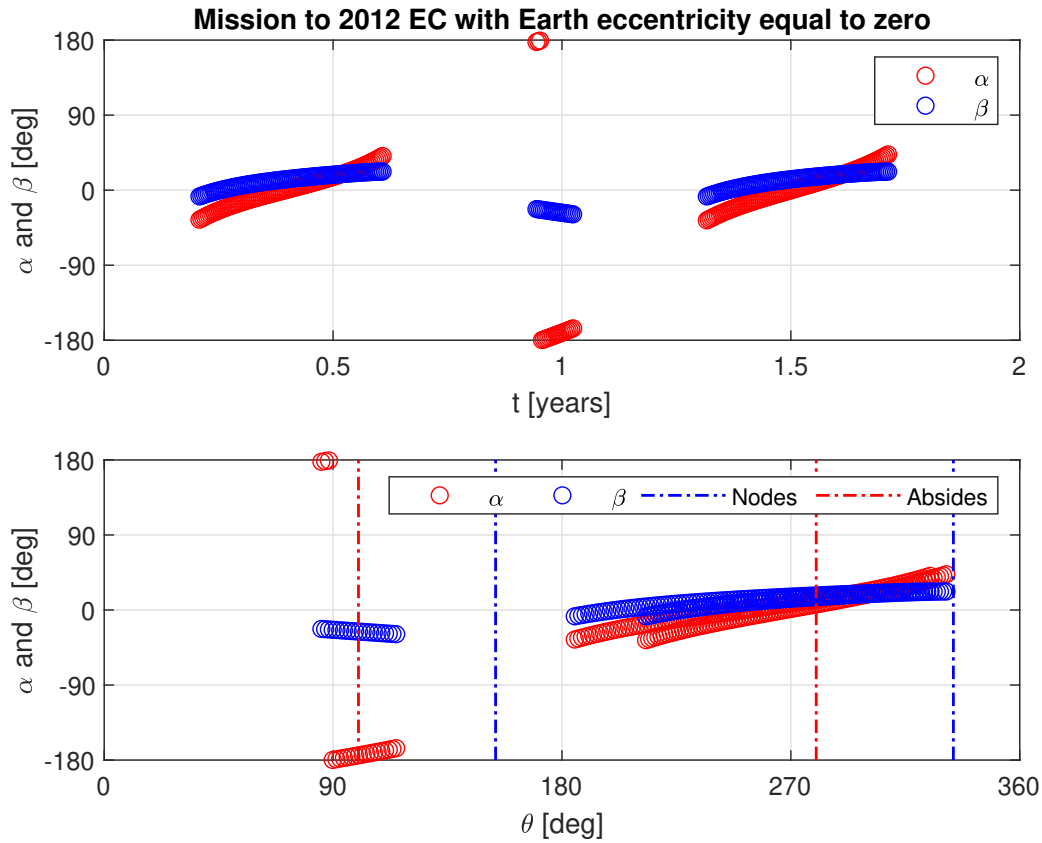
Figure 7.17: Trends of alpha, beta and theta for 2012 EC with $e_{Earth} = 0$.

It is possible to notice that, in this case, the engine firings occur with a higher regularity, thus demonstrating the eccentricity's influence on the type of optimum transfer. Looking at the longitudes at which engine firings occur, this last, for type B asteroid, is still taking place both on the absides line and nodes line, as this phenomenon is likely determined by high inclinations, which have not been varied to perform this simulation.

The last series of graphs reported below, shows the trends of angles alpha, beta and theta with variable inclinations, in cases of the aforementioned asteroids (2016 CF137 and 2012 EC). In the first four graphs, it is possible to notice how decreasing the inclination of asteroids' orbits, the engine firings intervals become more and more regular, with mean values of alpha for each firing interval being closer and closer to a null value.

The second two series of graphs are perhaps the most significant in this hypotheses testing procedure. In fact, it is clear in missions toward both asteroids that an increasing value of the inclination leads to a higher number of engine firings in positions close to the line of nodes while reducing the firings occurring on the lines of absides (the blue vertical straight lines indicate the angular position of nodes, while the red ones indicate the absides angular positions).
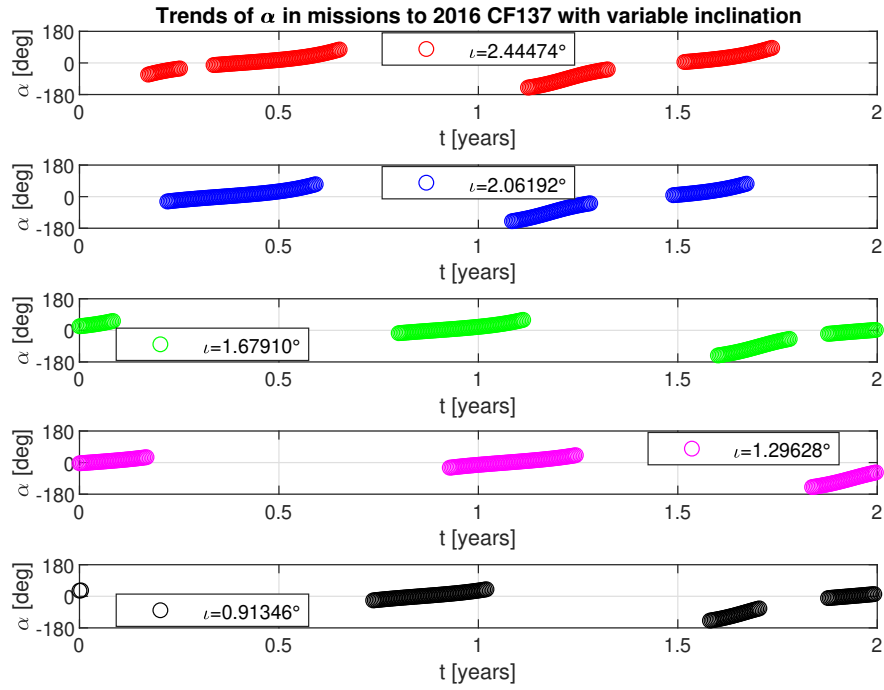
Figure 7.18: Trends of alpha for 2016 CF137 with variable inclination.
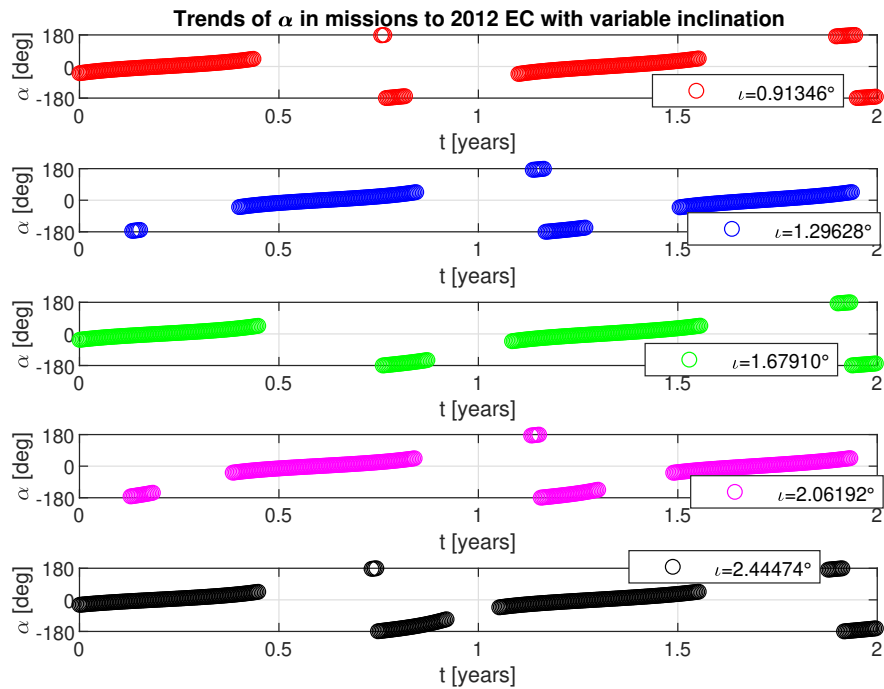

Figure 7.19: Trends of alpha for 2012 EC with variable inclination.
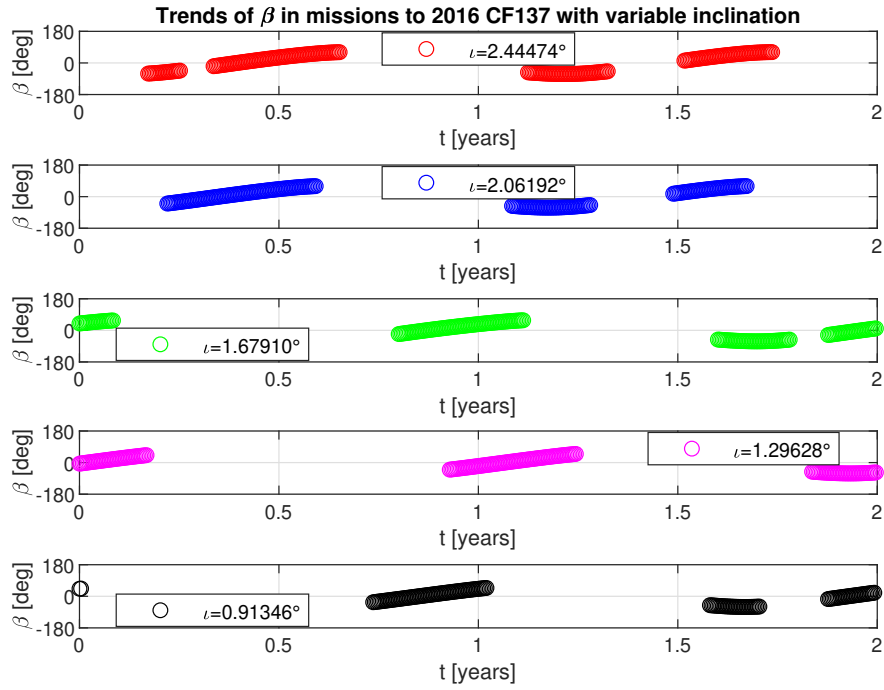
Figure 7.20: Trends of beta for 2016 CF137 with variable inclination.
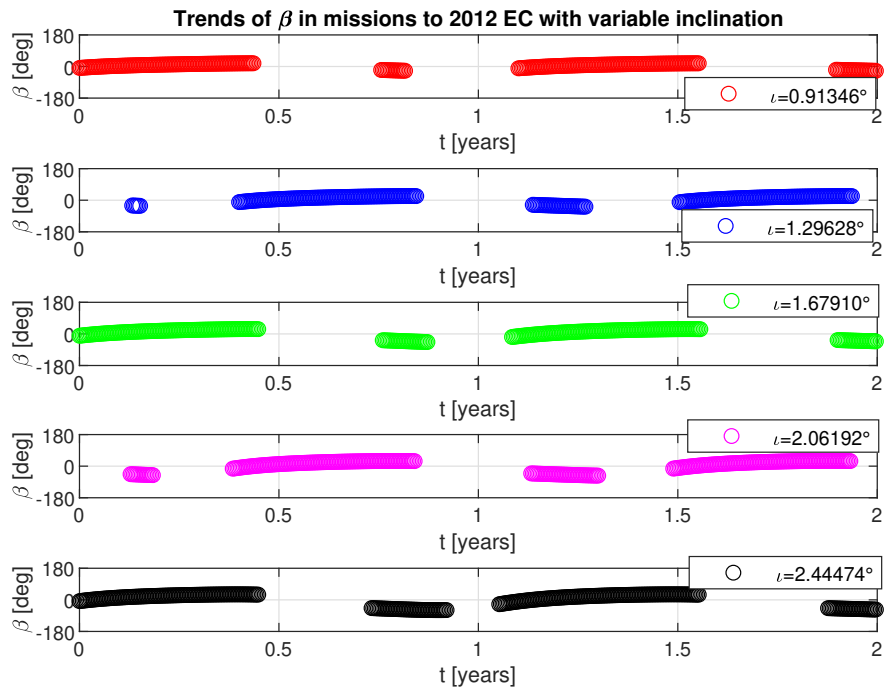
Figure 7.21: Trends of beta for 2012 EC with variable inclination.
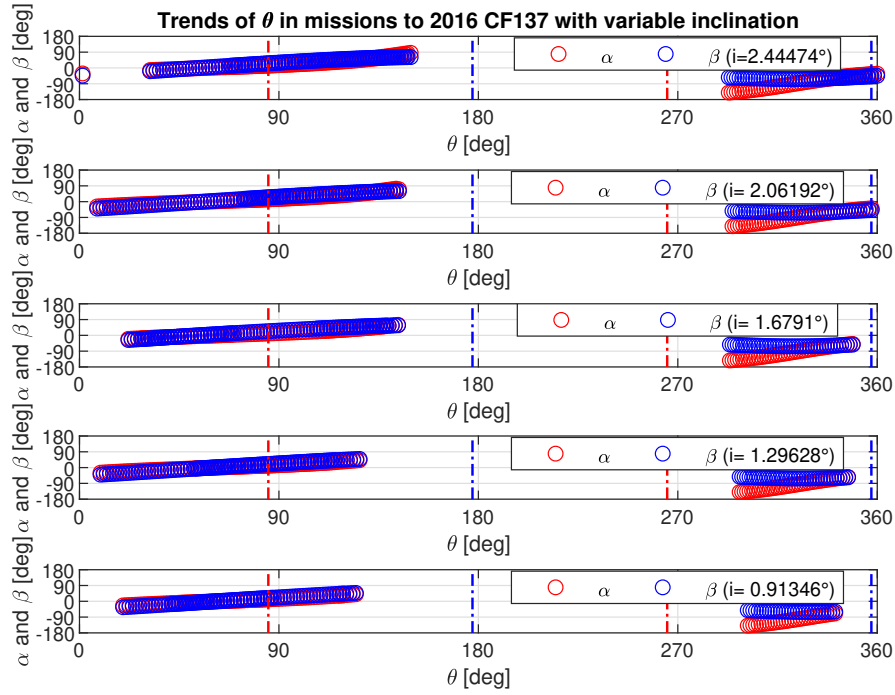
Figure 7.22: Trends of theta for 2016 CF137 with variable inclination.
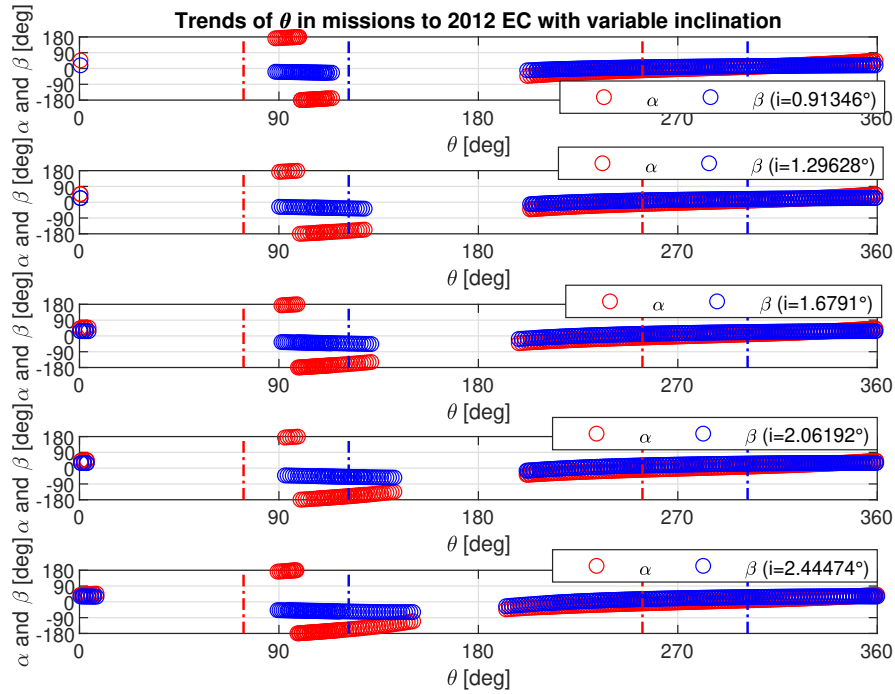
Figure 7.23: Trends of theta for 2012 EC with variable inclination.

Chapter 8

Conclusions

The work summarized in this thesis has shown and demonstrated that a particular combination of orbital parameters can lead to different strategies for missions if electric propulsion is assumed to be employed. In fact, missions toward ten Near-Earth asteroids have been simulated, solving the characteristic equations with indirect methods and considering only the heliocentric phase. Later observing some peculiar phenomena occurring to angles α and β when missions toward asteroids with mutual characteristics were simulated, with a constrained duration of two years, a series of three hypotheses have been formulated. In order to confirm and demonstrate or reject them, missions toward the same asteroids fictitiously modified have been simulated, thus giving evidence that by increasing or decreasing the parameters hypothesized to originate the observed differences, the same differences disappeared or became more evident, respectively. Therefore the initial hypotheses have been confirmed.

Possible future improvements of this work may focus on simulation of missions toward a higher number of Near-Earth asteroids, in order to verify if the conclusions given in this work can be true and extended to all asteroids orbiting in near-Earth environment. Moreover, it would be interesting to change the constrained duration of the missions, increasing but also decreasing the duration, to explore the feasibility of shorter missions and the changes of the results in longer missions.

Bibliography

[1] Abolfazl Shirazia, Josu Ceberio, and Jose A. Lozano, "Spacecraft trajectory optimization: A review of models, objectives, approaches and solutions" *Progress in Aerospace Sciences 102*, pp. 76–98, 2018.

[2] L. Casalino, "Ottimizzazione indiretta di traiettorie spaziali".

[3] Lorenzo Casalino, and Matthew A. Vavrinay, "Optimal power partitioning for electric thrusters".

[4] NASA/JPL-Caltech, "Asteroid Watch: Keeping an Eye on Near-Earth Objects", URL: https://www.jpl.nasa.gov/asteroid-watch.

[5] A. Morbidelli, "Origin and evolution of Near-Earth asteroids".

[6] D. F. Lupishko and M. Di Martino, "Physical properties of near-Earth asteroids", 1997.

[7] William F. Bottke Jr., Robert Jedicke, Alessandro Morbidelli, Jean-Marc Petit, Brett Gladman , "Understanding the Distribution of Near-Earth Asteroids".

[8] Niklas Anthony , M. Reza Emami, "Asteroid engineering: The state-of-the-art of Near-Earth Asteroids" *Progress in Aerospace Sciences 100* , pp. 1–17, 2018.

[9] NASA/JPL-Caltech, "PIA02923: Mosaic of Eros' Northern Hemisphere", URL: https://photojournal.jpl.nasa.gov/catalog/PIA02923.

[10] D. Farnocchia, S.R. Chesley, D. Vokrouhlicky, A. Milani, F. Spoto, W.F. Bottke, "Near Earth Asteroids with measurable Yarkovsky effect" *Icarus 224*, pp. 1–13, 2013.

[11] D.S. Lauretta, S.S. Balram-Knutson, E. Beshore, W.V. Boynton, "OSIRIS-REx: Sample Return from Asteroid (101955) Bennu", *Springer Science+Business Media B.V.*, 2017.

[12] Dmitrij Lupishko, Iryna Tielieusova, "Influence of the YORP effect on rotation rates of near-Earth asteroids" *Meteoritics & Planetary Science 49, Nr 1*, pp. 80–85, 2014.

[13] B. Rozitis, and S. F. Green, "The strength and detectability of the YORP effect in near-Earth asteroids: a statistical approach" *MNRAS 430*, pp. 1376–1389, 2013.

[14] Roger R. Bate, Donald D. Mueller, Jerry E. White, "Fundamentals of astrodynamics", *Dover publications, Inc.*, 1971.

[15] Kumari, Amisha & Deohans, Aayushi, "Orbital Lifetime Analysis of GTO Objects", 2019.

[16] J. W. Cornelisse, H.F.R. Schoeyer, K. F. Wakker, "Rocket propulsion and spaceflight dynamics", *Pitman publishing*, 1979.

[17] Robert G. Jahn, "Physics of electric propulsion", *McGraw-Hill, Inc.*, 1968.

[18] L. Casalino, "Space propulsion".

[19] L. Casalino, "Equazioni in coordinate sferiche".